

# ADDITIVE POLYNOMIAL METHODS, PART I: FRAMEWORK AND FULLY-IMPLICIT BLOCK METHODS \*

TOMMASO BUVOLI<sup>†</sup> AND BEN S. SOUTHWORTH<sup>‡</sup>

**Abstract.** In this paper we generalize the polynomial time integration framework to additively partitioned initial value problems. The framework we present is general and enables the construction of many new families of additive integrators with arbitrary order-of-accuracy and varying degree of implicitness. In this first work, we focus on a new class of implicit-explicit polynomial block methods that are based on fully-implicit Runge-Kutta methods with Radau nodes. We show that the new integrators have improved stability compared to existing IMEX Runge-Kutta methods, while also being more computationally efficient due to recent developments in preconditioning techniques for solving the associated systems of nonlinear equations. For PDEs on periodic domains where the implicit component is trivial to invert, we will show how parallelization of the right-hand-side evaluations can be exploited to obtain significant speedup compared to existing serial IMEX Runge-Kutta methods. For parallel (in space) finite-element discretizations, the new methods obtain accuracy several orders of magnitude lower than existing IMEX Runge-Kutta methods, and/or obtain a given accuracy as much as 16 times faster in terms of computational runtime.

**Key words.** Time-Integration, Additive Integrators, Semi-linear, Implicit-Explicit, Fully-implicit Runge-Kutta, Polynomial Block Methods

**AMS subject classifications.** 65L04, 65L05, 65L06

**1. Introduction.** Many problems in science and engineering can be modeled using high-dimensional systems of ordinary differential equations arising from the mathematical description of physical phenomena or from the spatial discretization of partial differential equations. Solving these systems amounts to integrating an initial value problem (IVP)

$$(1.1) \quad y'(t) = f(t, y(t)), \quad y(t_0) = y_0.$$

In practice, it is common to additively partition the right-hand-side,  $f(t, y)$ , into  $m$  components,

$$(1.2) \quad f(t, y) = \sum_{j=1}^m f^{\{j\}}(t, y).$$

A simple example is a discretized advection-diffusion-reaction equation where each physical process is represented by a separate term.

The solution of any additively partitioned system can be numerically approximated using an additive integrator that treats each component  $f^{\{j\}}(t, y)$  differently [22, 31, 37]. This can be particularly efficient for solving multiscale, multiphysics problems where the optimal method differs across the components, or where it is prohibitively expensive to treat the full operator  $f(t, y)$  implicitly. A canonical example is a linear advection-diffusion equation, where the diffusion places severe explicit time-step restrictions, but fully implicit solves for advection-diffusion discretizations

\*Submitted to the editors DATE.

**Funding:** BSS was supported as a Nicholas C. Metropolis Fellow under the Laboratory Directed Research and Development program of Los Alamos National Laboratory.

<sup>†</sup>Department of Applied Mathematics, University of California, Merced, Merced CA 95343, USA. (tbuvoli@ucmerced.edu).

<sup>‡</sup>Theoretical Division, Los Alamos National Laboratory, USA (southworth@lanl.gov).

are significantly more challenging than for pure diffusion. An additive integrator can treat the diffusion implicitly and the advection explicitly, addressing each of these problems. If the right-hand-side consists of two components and an additive integrator treats the first implicitly and the second explicitly, then the integrator is frequently called an implicit-explicit (IMEX) method.

Two closely related classes of integrators are semi-implicit methods and W-methods, that respectively utilize an exact or approximate local Jacobian of  $f(t, y)$  at each timestep [43, IV.7][15, 1, 26]. Given the solution at the  $n$ th timestep  $y_n = y(t_n)$ , we can rewrite the system (1.1) as an additively partitioned system with  $m = 2$ ,

$$(1.3) \quad f^{\{1\}}(t, y) = J_n y, \quad \text{and} \quad f^{\{2\}}(t, y) = f(t, y) - J_n y,$$

where  $J_n$  approximates or is equal to the local Jacobian  $\frac{\partial f}{\partial y}(y_n)$ . Any additive integrator that treats  $f^{\{1\}}(t, y)$  implicitly and  $f^{\{2\}}(t, y)$  explicitly reduces to a semi-implicit method.

In the past three decades, the construction of additive integrators has been an active area of research that has produced a range of methods, including linear multistep methods (LMMs) [6, 23, 42], Runge-Kutta (RK) methods [5, 31, 34, 37, 29, 32], and general linear methods (GLMs) [17, 45, 39], including those based on extrapolation [21, 16]. Each method class has certain benefits and drawbacks. Additive LMMs have a low computational cost per timestep, but high-order methods experience instabilities on equations with limited diffusion. Additive diagonally implicit RK methods possess good stability and allow for simplified adaptive time-stepping, however they are known to suffer from order-reduction on stiff equations [7]. Moreover, high-order RK method derivations that rely on nonlinear order conditions grow increasingly difficult to construct, and alternative approaches must be considered [21, 34]. GLMs with good stability and no order-reduction have been derived, however to avoid increasing the number of order conditions further, one must typically consider simplified method formulations.

In this paper we will generalize the recently introduced polynomial time integration framework [9, 14, 10, 13] to include additively partitioned differential equations, and demonstrate its utility by introducing several new method families. There are two main advantages of the additive polynomial framework that will be explored in this paper. First, the framework simplifies the construction of high-order additive GLMs that do not suffer from order-reduction on stiff equations. Specifically, the polynomial framework makes extensive use of interpolating polynomials that trivially satisfy nonlinear order conditions and ensure high stage-order. Furthermore, method construction can be done using geometric arguments that are similar to those used to derive spatial finite difference stencils. Second, the framework can be used to derive efficient methods for solving equations that are either naturally split into multiple terms, or where the right-hand-side has been rewritten using an exact or approximate Jacobian. This allows us to simultaneously introduce a range of new high-order additive and semi-implicit integrators.

The additive polynomial framework we present is very general. Therefore when discussing method construction we will focus exclusively on the special case of implicit-explicit methods. Moreover, we will only present a single new family of methods that are based on fully-implicit Runge-Kutta integrators. This choice may seem peculiar since fully-implicit methods are often considered too slow to be competitive. However, recent developments in block linear and nonlinear solvers make their use in numerical PDEs quite tractable [18, 35, 25, 30, 36, 41, 40], even outperforming diagonally implicit

RK methods in many cases [41, 40]. Despite these developments, it is not possible to derive IMEX RK methods based on the fully implicit RK methods since the explicit stages would be nonlinearly coupled to the fully implicit stages. More generally, constructing high order IMEX RK or GLM schemes is often nontrivial, as mentioned in [32]. In this work, we will show how the polynomial framework provides a natural way to develop fully-implicit-explicit integrators, which are naturally high-order accurate, and allow us to leverage developments in fully implicit solvers in the context of additive integration.

This paper is organized as follows. In Sections 2 and 3 we respectively provide short introductions to additive integrators and the polynomial framework. In Section 4 we generalize the polynomial framework for additively partitioned differential equations, and in Section 5 we develop new classes of fully-implicit-explicit methods and study their stability. Section 6 demonstrates the improved accuracy and efficiency of the new integrators in practice, often achieving orders of magnitude lower error than comparable IMEX-RK methods, with comparable computational runtimes.

**2. Additive integrators.** Additive integrators are a class of methods for solving the partitioned initial value problem (1.1, 1.2). In this section, we give a short introduction to additive integrators for equations with two partitions ( $m = 2$ ), where

$$(2.1) \quad y' = f^{\{1\}}(t, y) + f^{\{2\}}(t, y), \quad y(t_0) = y_0.$$

We assume that the term  $f^{\{1\}}(t, y)$  is stiff (i.e. a small stepsize is required for any explicit method when solving  $y' = f^{\{1\}}(t, y)$ ) while the term  $f^{\{2\}}(t, y)$  is nonstiff.

In such a scenario it is desirable to consider integrators that only treat  $f^{\{1\}}(t, y)$  implicitly. One approach for deriving additive methods is to integrate (2.1), and then approximate the resulting integrals for each term separately

$$(2.2) \quad y(t_{n+1}) = y(t_n) + \underbrace{\int_{t_n}^{t_{n+1}} f^{\{1\}}(t, y(t)) dt}_{\text{treat implicitly}} + \underbrace{\int_{t_n}^{t_{n+1}} f^{\{2\}}(t, y(t)) dt}_{\text{treat explicitly}}.$$

One of the simplest additive integrators can be derived by taking an implicit one-sided approximation for  $f^{\{1\}}(t, y)$ , and an explicit one-sided approximation for  $f^{\{2\}}(t, y)$ . This produces the IMEX Euler method

$$(2.3) \quad y_{n+1} = y_n + hf_{n+1}^{\{1\}} + hf_n^{\{2\}},$$

where the stepsize  $h = t_{n+1} - t_n$ . Higher-order IMEX-LMM methods [6, 23] use higher-order polynomial approximations constructed from previous solution values, while the output of a higher-order IMEX-RK method [5, 31, 37, 32] is a linear combination of newly computed stage values. IMEX-GLMs [17, 45, 39] combine both ideas by using previous solution values and new stages.

When using any IMEX method there are a range of choices for  $f^{\{1\}}$  and  $f^{\{2\}}$  that affect the computational cost and stability of the integrator. For a semi-linear system  $y' = Ly + N(t, y)$ , with a nonstiff nonlinearity, it is natural to let

$$(2.4) \quad f^{\{1\}}(t, y) = Ly, \quad f^{\{2\}}(t, y) = N(t, y).$$

For a more general nonlinear system  $y' = A(t, y) + B(t, y)$  several choices include:

1. Fully implicit in  $A(t, y)$ :

$$(2.5) \quad f^{\{1\}}(t, y) = A(t, y), \quad f^{\{2\}}(t, y) = B(t, y).$$

2. Linearly implicit in  $A(t, y)$ :

$$(2.6) \quad f^{\{1\}}(t, y) = \frac{\partial A}{\partial y}(t_n, y_n), \quad f^{\{2\}}(t, y) = B(t, y) + A(t, y) - \frac{\partial A}{\partial y}(t_n, y_n).$$

3. Linearly implicit in  $A(t, y)$  and  $B(t, y)$ :

$$(2.7) \quad \begin{aligned} f^{\{1\}}(t, y) &= \frac{\partial A}{\partial y}(t_n, y_n) + \frac{\partial B}{\partial y}(t_n, y_n), \\ f^{\{2\}}(t, y) &= B(t, y) + A(t, y) - \frac{\partial A}{\partial y}(t_n, y_n) - \frac{\partial B}{\partial y}(t_n, y_n). \end{aligned}$$

4. Linearly implicit in  $J_n$ : ( $J_n$  approximates the full or partial Jacobian at  $t = t_n$ )

$$(2.8) \quad f^{\{1\}}(t, y) = J_n y, \quad f^{\{2\}}(t, y) = B(t, y) + A(t, y) - J_n y.$$

For additional clarity we write the formulas for the IMEX-Euler method using three of the proposed partitionings:

$$\begin{aligned} \text{partitioning (2.4)} \quad & y_{n+1} = (I - hL)^{-1}(y_n + hN(t_n, y_n)), \\ \text{partitioning (2.5)} \quad & y_{n+1} = y_n + hA(t_{n+1}, y_{n+1}) + hB(t_n, y_n), \\ \text{partitioning (2.8)} \quad & y_{n+1} = y_n + (I - hJ_n)^{-1}h(B(t_n, y_n) + A(t_n, y_n)). \end{aligned}$$

Selecting a fully implicit partitioning generally leads to improved stability but requires a nonlinear solve at each timestep. Conversely, a linearly implicit choice only requires a linear solve at each step, but the method may have inferior stability properties, especially if  $J_n$  does not closely approximate the local Jacobian.

In the sections that follow we will first review the polynomial time integration framework, and then generalize it so that we can construct new high-order additive integrators for (2.3) using any of the proposed partitionings (2.4)-(2.8).

**3. Polynomial time integrators.** The polynomial time integration framework [9, 14] is based on continuous polynomials in time that are constructed by fitting through solution or derivative values. The values may be known (i.e input values) or unknown (i.e. future stage values or outputs), with the latter leading to implicit equations and ultimately implicit methods. Within the family of classical time integration methods, we can interpret polynomial time integrators as parametrized GLMs whose inputs and outputs approximate the solution at a set of scaled nodes  $\{z_j\}$  where the scaling factor is called the *node radius*  $r$ . Note that the node radius introduces an additional degree of freedom that complements the stepsize  $h$ .

The input and output values of a polynomial integrator, along with the associated derivatives, are represented using the notation

$$\begin{aligned} \text{input (solutions):} \quad & y_j^{[n]} \approx y(t_n + rz_j) \\ \text{output (solutions):} \quad & y_j^{[n+1]} \approx y(t_n + rz_j + h) \\ \text{input derivatives:} \quad & f_j^{[n]} := f(t_n + rz_j, y_j^{[n]}) \approx y'(t_n + rz_j) \\ \text{output derivatives:} \quad & f_j^{[n+1]} := f(t_n + rz_j + h, y_j^{[n+1]}) \approx y'(t_n + rz_j + h). \end{aligned}$$

The name polynomial integrator originates from the fact that all the method coefficients are derived using interpolating polynomials, known as *ODE polynomials*.

All ODE polynomials approximate the Taylor series of the solution in local coordinates  $\tau$ , where

$$(3.1) \quad t(\tau) = r\tau + t_n.$$

The general form for an ODE polynomial of degree  $g$  with expansion point  $b$  is

$$(3.2) \quad p(\tau; b) = \sum_{j=0}^g \frac{a_j(b)(\tau - b)^j}{j!}$$

where the constants  $\{a_j(b)\}$  are called *approximate derivatives* since they approximate the derivatives of the solution in local coordinates such that  $a_j(b) \approx \left. \frac{d^j}{d\tau^j} y(t(\tau)) \right|_{\tau=b} = r^j y^{(j)}(t(b))$  (the factor of  $r$  originates from the transformation into local coordinates (3.1)). Each approximate derivative  $a_j(b)$  is computed by differentiating interpolating polynomials that are constructed using any subset of the method's inputs, outputs, stages, and the corresponding derivatives. The order of the polynomial method is directly related to the degree of its ODE polynomials and the order of the interpolating polynomials that are used to construct the associated approximate derivatives [9, Sec. 3.6]. As a consequence, the order of accuracy is always bounded below by  $\min(g_{min}, \delta - 1)$  where  $g_{min}$  is the minimum degree of the ODE polynomials and  $\delta$  is the minimum degree of all the polynomials that determine the approximate derivatives.

A general formulation for the approximate derivatives  $a_j(b)$  is described in [9, 14]; here we will only describe two important sub-families:

1. *Adams ODE polynomials* are constructed using two Lagrange interpolating polynomials  $L_y(\tau)$  and  $L_f(\tau)$  that respectively satisfy solution values or derivative values at the method's input, output, or stage nodes. Specifically,  $L_y(\tau) \approx y(t(\tau))$  interpolates at least one solution value, and  $L_f(\tau) \approx ry'(t(\tau))$  is a polynomial of degree  $g - 1$  that interpolates  $g$  derivative values. The approximate derivatives are then

$$(3.3) \quad a_0(b) = L_y(b), \quad \text{and} \quad a_j(b) = \frac{d^{j-1} L_f}{d\tau^{j-1}}(b), \quad j = 1, \dots, g.$$

By substituting (3.3) into (3.2) and noting that  $p'(\tau; b) = L_f(\tau)$ , we can express an Adams ODE polynomial in the equivalent integral form

$$(3.4) \quad p(\tau; b) = L_y(b) + \int_b^\tau L_f(\xi) d\xi.$$

We now see that an Adams ODE polynomial approximates the integral equation of an initial value problem where the expansion point  $b$  is the location of the initial condition in local coordinates.

2. *BDF ODE polynomials* are constructed using a polynomial  $H_y(\tau) \approx y(t(\tau))$  of degree  $g$  that interpolates  $g$  solution values and whose derivative  $H'_y(\tau)$  interpolates a single derivative value. The approximate derivatives are given by

$$(3.5) \quad a_j(b) = \frac{d^j H}{d\tau^j}(b) \quad \implies \quad p(\tau; b) = H(\tau) \quad \forall b.$$

Note that BDF polynomials do not depend on the expansion point  $b$ .

Since ODE polynomials are expressed in local coordinates (3.1), it is convenient to also parametrize the stepsize  $h$  in terms of the node radius. We therefore let

$$(3.6) \quad h = r\alpha$$

where the constant  $\alpha$  is called the *extrapolation factor*. In Figure 1 we show a visualization of the parameters  $r$ ,  $h$ , and  $\alpha$  for a method with three real-valued, equispaced nodes  $\{z_j\}$ .

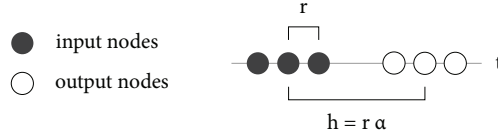


**Fig. 1:** A visualization of the input and output nodes for a polynomial integrator with  $q = 3$  and nodes  $z_j = \{-1, 0, 1\}$ . The node set is scaled by the node radius and the distance between the inputs and outputs is proportional to the extrapolation factor  $\alpha$ .

When presenting polynomial methods, it is convenient to introduce a set containing all the data values that can be used to construct the interpolating polynomials that determine the approximate derivatives  $a_j(b)$  in the ODE polynomial (3.2). This set is called the *ODE dataset*, and in the case of classical polynomial methods, it simply contains the method's inputs, outputs, stages, and their derivatives, along with the corresponding temporal nodes. An ODE dataset of size  $w$  is denoted as

$$(3.7) \quad D(r, t_n) = \{(\tau_j, y_j, r f_j)\}_{j=1}^w \quad \text{where} \quad y_j \approx y(t(\tau_j)), \quad f_j = f(t(\tau_j), y_j).$$

Using all the previous definitions, the formula for any polynomial method with  $s$  stages and  $q$  outputs can be written compactly as

$$(3.8) \quad \begin{aligned} Y_i &= p_j(c_j(\alpha), b_j(\alpha)) & j &= 1, \dots, s, \\ y_j^{[n+1]} &= p_{j+s}(z_j + \alpha; b_{j+s}(\alpha)) & j &= 1, \dots, q, \end{aligned}$$

where  $Y_i$  denote stage values,  $c_j(\alpha)$  are stage nodes in local coordinates, and  $p_j(\tau; b)$  are ODE polynomials constructed from an ODE dataset of size  $w = 2q + s$  that contains the methods inputs, stage values, and outputs. The associated temporal nodes of the method's ODE datasets (3.7) are respectively

$$(3.9) \quad \tau_j = \begin{cases} z_j & 1 \leq j \leq q, \\ c_{j-q}(\alpha) & q + 1 \leq j \leq q + s, \\ z_{j-q-s} + \alpha & q + s < j \leq 2q + s. \end{cases}$$

In this work we look at methods with real-valued quadrature nodes  $\{z_j\}$  that are scaled relative to the interval  $[-1, 1]$ . This choice is inspired by the fact that nearly all of the theoretical analysis relating to orthogonal polynomials and interpolation is conducted on this interval. However, when implementing a polynomial integrator it is typically simpler to translate the nodes to the interval  $[0, 2]$  such that the left-most node at  $\tau = 0$  is located at  $t = t_0$  where the initial condition for (1.1) is provided. Translating the nodes only affects temporal locations of the inputs, as determined by (3.1), and has no effect on the method coefficients.

Using the general formulation (3.8), it is possible to derive many different families of polynomial integrators. One example is *polynomial block methods* (PBMs) from [14] which are characterized by  $s = 0$  and will be the primary focus of this paper due to their simpler structure. Additional examples include well-known time integrators like backward difference formulas (BDF), Adams-Moulton methods, and collocation methods, which can all be expressed as polynomial-based methods with a fixed  $\alpha$ . In the following subsection we show how to write fully implicit collocation methods in the polynomial framework. The resulting formulation will be used again in Section 5 to construct new additive polynomial integrators.

**3.1. Collocation methods and Radau IIA.** Collocation methods [27, II.7] are time integrators based on polynomial quadrature that can also be expressed as fully-implicit Runge-Kutta methods. Well-known examples include the A-stable Gauss methods [8, Sec. 342] and the L-stable Radau IIA methods [28] that respectively achieve orders of  $2m$  and  $2m - 1$ , where  $m$  is the number of stages.

Suppose that we seek an approximate solution of (1.1) at  $t = t_n + h$  given an initial condition  $y_n = y(t_n)$ . To derive a collocation method, we can approximate the solution  $y(t)$  using a polynomial  $p_y(t)$  that satisfies the initial condition at  $t = t_n$  and the differential equation at a set of  $m$  collocation points  $t_{n,j}$  such that  $p'_y(t_{n,j}) = f(t_{n,j}, p_y(t_{n,j}))$ . These constraints lead to the fully-implicit nonlinear system

$$(3.10) \quad p_y(t_{n,j}) = y_n + \int_{t_n}^{t_{n,j}} \underbrace{\sum_{j=1}^m \ell_j(t) F(t_{n,j}, p_y(t_{n,j}))}_{p_f(t)} dt, \quad j = 1 \dots, m$$

where  $\ell_j(t) = \prod_{k \neq j} (t - t_{n,k}) / (t_{n,j} - t_{n,k})$  is the  $j$ th Lagrange basis polynomial and  $p_f(t)$  is a Lagrange interpolating polynomial for the solution derivative  $y'(t)$ . If we compare the right-hand-side of (3.10) to the Adams ODE polynomial integral formulation (3.4), we see that  $p_y(t(\tau))$  is equivalent to an Adams ODE polynomial  $p(\tau; b)$  with  $b = t(t_n)$ ,  $L_y(\tau) = y_n$ , and  $L_F(\tau) = p_f(t(\tau))$ . Therefore, by appropriately defining an ODE dataset and node set  $\{z_j\}$  we can express any collocation method (3.10) as a one-step polynomial integrator with  $q = 1$ ,  $s = m$ , and whose output is computed using a single Adams ODE polynomial.

However, for the purposes of this paper we will instead rewrite a collocation method as a multivalued PBM, where we advance the full “block” solution at the set of collocation points forward in time by  $h$ . To simplify the derivation we focus solely on a Radau IIA method with  $\sigma - 1$  stages, and show how this integrator can be re-expressed as a PBM with fixed  $\alpha$  and  $q = \sigma$ . Though such a formulation may seem unnecessarily verbose, we will use the multivalued inputs (i.e., solutions at collocation points from the previous time step) in Section 5 to construct a new class of additive IMEX integrators.

We start by selecting the PBM nodes

$$(3.11) \quad \{z_j\}_{j=1}^q = \{-1, 2x_1 - 1, \dots, 2x_{q-1} - 1\},$$

where  $x_j$  is the  $j$ th zero of the polynomial  $\frac{d^{q-2}}{dx^{q-2}}(x^{q-2}(x-1)^{q-1})$ . Our first quadrature node is  $z_1 = -1$  and the remaining nodes are the  $q - 1$  Radau nodes scaled on the interval  $x \in [-1, 1]$ . In Figure 2(a), we illustrate the input and output nodes for a method with  $q = 3$ .

The outputs of the PBM will all be computed using a single Adams ODE polynomial (3.4). Since we want a method based on implicit Radau quadrature, we select

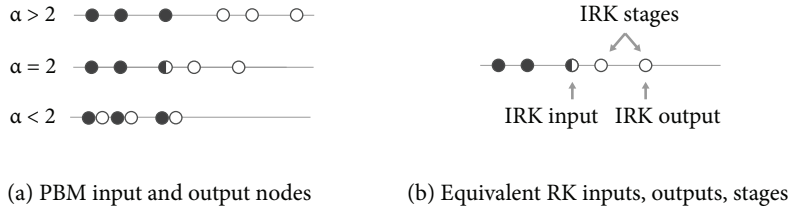


**Fig. 2:** Illustration of input nodes  $\bullet$  and output nodes  $\circ$  for the PBM with nodes (3.11) and  $q = 3$ , such that  $\{z_j\} = \{-1, -1/3, 1\}$ . The grey lines show the time axis which flows to the right. (a) An illustration of the temporal nodes for the input and outputs for three different values of  $\alpha$ . When  $\alpha = 2$  the last input node overlaps with the first output node. (b) A depiction showing how the inputs and outputs of the PBM (3.12) with  $b = 1$  and  $\alpha = 2$  relate to the the input, output, and stage values of an IRK method at the  $n$ th timestep.

$L_f(\tau)$  to be the interpolating polynomial that matches all the output derivatives at the scaled Radau nodes ( $L_f(z_j + \alpha) = f_j^{[n+1]}$  for  $j = 2, \dots, q$ ). To maximize the accuracy of the integration constant  $L_y(b)$  we choose  $L_y(\tau)$  to be the interpolating polynomial that matches all the input values ( $L_y(z_j) = y_j^{[n]}$  for  $j = 1, \dots, q$ ). If we temporarily leave the expansion point  $b$  free, then we obtain the PBM

$$(3.12) \quad y_j^{[n+1]} = p(z_j + \alpha; b) = L_y(b) + \int_b^{z_j + \alpha} L_f(s) ds, \quad j = 1 \dots, q.$$

To obtain a one-step Radau IIA collocation we:

1. Select  $\alpha = 2$ . The last input node now overlaps with the first output node; see Figure 2(a). This allows us to use the last input value as an accurate integration constant for Radau quadrature.
2. Select  $b = 1$ . This choice sets the last input  $y_q^{[n]}$  as the integration constant since  $L_y(1) = y_q^{[n]}$ . Furthermore,  $y_1^{[n+1]} = p(z_1 + 2; 1) = y_q^{[n]}$ , therefore the first output is equal to the last input.

The resulting PBM is equivalent to a  $(2q - 3)$ th order, one-step Radau IIA collocation method with stepsize  $h = 2r$ . Note that for general  $b$  and  $\alpha$ , the PBM (3.12) is a  $(q - 1)$ th order, fully-implicit multivalued integrator<sup>1</sup>.

We can relate the inputs and outputs of the PBM with  $\alpha = 2$  and  $b = 1$  to the RK inputs and stages according to the following Table which is also visualized in Figure 2(b):

RK step index $\nu$	RK input $y_\nu$	RK output $y_{\nu+1}$	RK stages
$n - 1$	$y_{n-1} = y_1^{[n]}$	$y_n = y_q^{[n]}$	$Y_{j-1} = y_j^{[n]}, j = 2, \dots, q$
$n$	$y_n = y_q^{[n]}$	$y_{n+1} = y_q^{[n+1]}$	$Y_{j-1} = y_j^{[n+1]}, j = 2, \dots, q$

For clarity we write the PBM for  $q = 3$ . The nodes are  $\{z_j\} = \{-1, -1/3, 1\}$ ,

<sup>1</sup>Regardless of the fact that we have Radau nodes, selecting general  $b$  will not produce a method with  $2\sigma - 3$  accuracy. This is due to the fact that our initial condition will only be order  $q - 1$  accurate, and the lower integration bound is different than the one used for Radau quadrature.



and the polynomials are

$$\begin{aligned} L_y(\tau) &= \frac{(t-1)(3t+1)}{4} y_1^{[n]} - \frac{9(t^2-1)}{8} y_2^{[n]} + \frac{(t+1)(3t+1)}{8} y_3^{[n]}, \\ L_f(\tau) &= -\frac{3}{4} (\tau - \alpha - 1) r f_2^{[n+1]} + \frac{3}{4} (\tau - \alpha + \frac{1}{3}) r f_3^{[n+1]}. \end{aligned}$$

Selecting  $b = 1$  and  $\alpha = 2$ , and substituting  $L_y(\tau)$  and  $L_f(\tau)$  into (3.12) yields

$$(3.13) \quad \begin{aligned} y_1^{[n+1]} &= y_3^{[n]} \\ y_2^{[n+1]} &= y_3^{[n]} + \frac{5}{6} r f_2^{[n+1]} - \frac{1}{6} r f_3^{[n+1]} \\ y_3^{[n+1]} &= y_3^{[n]} + \frac{3}{2} r f_2^{[n+1]} + \frac{1}{2} r f_3^{[n+1]} \end{aligned}$$

which reduces to a Radau IIA method with stepsize  $h = 2r$  (replacing  $r$  with  $h/2$  produces the well-known IRK coefficients). Also note that the first two inputs are not used to compute the output, therefore this formula is equivalent to a one-step method.

**3.2. Iterators.** Before introducing additive integrators, we require one additional concept from the polynomial framework, namely the idea of an iterator. A polynomial integrator only advances the solution if the extrapolation factor  $\alpha$  is greater than zero (see Figure 1). If we let  $\alpha = 0$ , then we obtain a special method known as an iterator. Iterators recompute the solution at the current timestep and certain method constructions share many similarities with predictor corrector block methods [38] and spectral deferred correction iterations [24, 19]. In [13] iterators were used in the context of exponential integration to compute initial conditions and create composite methods with improved stability. In this work, we will show how these same ideas can be applied to additive polynomial integrators.

**4. Additive polynomial integrators.** In this section we introduce the additive polynomial time integration framework for solving the partitioned system

$$(4.1) \quad y'(t) = f(t, y(t)) = \sum_{j=1}^m f^{\{j\}}(t, y(t)).$$

In Subsection 4.1 we extend the ODE dataset (3.7) and the ODE polynomial (3.1) from the unpartitioned system (1.1) to the partitioned system (4.1). Then, in Subsection 4.2 we introduce the class of additive polynomial block methods that will provide a starting point for deriving new integrators in Section 5.

**4.1. Partitioned ODE datasets & ODE polynomials.** A partitioned ODE dataset contains all the data values that can be used to construct partitioned ODE polynomials. We can trivially extend the ODE dataset for partitioned equations by replacing the full right-hand-side  $f(t, y)$  with all the derivative components  $f^{\{j\}}(t, y)$ .

**DEFINITION 4.1** (Partitioned ODE Dataset). *A partitioned ODE dataset  $D(r, s)$  of size  $w$  is an ordered set of tuples of the form*

$$(4.2) \quad D(r, s) = \left\{ \left( \tau_j, y_j, r f_j^{\{1\}}, \dots, r f_j^{\{m\}} \right) \right\}_{j=1}^w$$

where  $t(\tau) = r\tau + s$ ,  $y_j \approx y(t(\tau_j))$ , and  $f_j^{\{k\}} = f^{\{k\}}(t(\tau_j), y_j)$ .

Before generalizing the ODE polynomial it is convenient to first introduce the notion of a *total derivative*.

DEFINITION 4.2 (Total Derivative). *A total derivative  $F$  approximates the local ODE solution derivative  $ry'(\tau)$  at a point  $\tau = \hat{\tau}$ , such that  $F \approx ry'(t(\hat{\tau}))$ , and is the sum of  $m$  derivative components, that is*

$$(4.3) \quad F = rf_{k_1}^{\{1\}} + rf_{k_2}^{\{2\}} + \dots + rf_{k_m}^{\{m\}} \quad \text{where} \quad \hat{\tau} = \tau_{k_1} = \tau_{k_2} = \dots = \tau_{k_m},$$

for indices  $k_l \in \{1, \dots, w\}$  and  $l = 1, \dots, m$ .

In words, a total derivative is the sum of  $m$  component derivatives from an ODE dataset where the  $j$ th component derivative approximates  $rf^{\{j\}}(t(\hat{\tau}), y(t(\hat{\tau})))$ .

To generalize the ODE polynomial for partitioned systems, we can reuse (3.2) and simply modify the rules for computing approximate derivatives.

DEFINITION 4.3 (Partitioned ODE Polynomial). *A partitioned ODE polynomial of degree  $g$  with expansion point  $b$  can be expressed as*

$$(4.4) \quad p(\tau; b) = \sum_{j=0}^g \frac{a_j(b)(\tau - b)^j}{j!},$$

where each approximate derivative  $a_j(b)$  is computed using values from a partitioned ODE dataset  $D(r, s)$  in one of the following ways:

1. By differentiating a polynomial  $h_j(\tau)$  that approximates  $y(t(\tau))$ ;  $h_j(\tau)$  must be a polynomial of least degree that interpolates at least one solution value in  $D(r, s)$  and whose derivative  $h'_j(\tau)$  interpolates any number of total derivatives from Definition 4.2. The  $j$ th approximate derivative of the ODE polynomial is then

$$a_j(b) = \left. \frac{d^j}{d\tau^j} h_j(\tau) \right|_{\tau=b}.$$

2. By differentiating a polynomial  $l_j(\tau)$  that approximates  $ry'(t(\tau))$ ;  $l_j(\tau)$  is formed by summing  $m$  Lagrange interpolating polynomials so that

$$l_j(\tau) = \sum_{k=1}^m l_j^{\{k\}}(\tau).$$

where  $l_j^{\{k\}}(\tau) \approx f^{\{k\}}(t(\tau), y(t(\tau)))$ . Each of the interpolating polynomials  $l_j^{\{k\}}$  must satisfy at least one of the derivative component values; specifically, for all  $k$  there exists at least one index  $\nu \in \{1, \dots, w\}$ , such that  $l_j^{\{k\}}(\tau_\nu) = rf_\nu^{\{k\}}$ . The  $j$ th approximate derivative is then

$$a_j(b) = \left. \frac{d^{j-1}}{d\tau^{j-1}} l_j(\tau) \right|_{\tau=b} \quad (\text{only valid for } j \geq 1).$$

When the number of components  $m = 1$ , the formulas for the approximate derivatives reduce to those of the classical ODE polynomials described in [14]. As is the case for classical ODE polynomials, the family of all additive ODE polynomials is large. Therefore, to simplify method construction, we focus on two special families that depend on significantly fewer free parameters.

**4.1.1. Special families of partitioned ODE polynomials.** We can generalize the Adams and BDF subfamilies (3.3) and (3.5) for the partitioned ODE polynomial (4.4). In particular:

1. A *partitioned Adams ODE polynomial* has approximate derivatives

$$(4.5) \quad a_j(b) = \begin{cases} L_y(b) & j = 0 \\ \frac{d^j}{d\tau^j} \sum_{k=1}^m L_f^{\{k\}}(\tau) \Big|_{\tau=b} & 1 \leq j \leq g \end{cases}$$

where:

- $L_y(\tau) \approx y(t(\tau))$  is a Lagrange interpolating polynomial that interpolates only solution data in  $D(r, s)$ ; specifically, for any number of distinct indices  $\nu \in \{1, \dots, w\}$ ,  $L_y(\tau_\nu) = y_\nu$ .
- Each  $L_f^{\{k\}}(\tau) \approx r f^{\{k\}}(t(\tau), y(t(\tau)))$  is a Lagrange interpolating polynomial of degree  $g - 1$  that satisfies  $g$  data values pertaining to the  $k$ th derivative component; specifically, for  $g$  distinct indices  $\nu \in \{1, \dots, w\}$ ,  $L_f^{\{k\}}(\tau_\nu) = r f_\nu^{\{k\}}$ .

Like the classical Adams ODE polynomial (4.6), all partitioned Adams ODE polynomials can be expressed in integral form as

$$(4.6) \quad p(\tau; b) = L_y(b) + \int_b^\tau \sum_{k=1}^m L_f^{\{k\}}(\xi) d\xi.$$

2. A *partitioned BDF ODE polynomial* has approximate derivatives that all satisfy

$$(4.7) \quad a_j(b) = \frac{d^j}{d\tau^j} H_y(\tau) \Big|_{\tau=b} \implies p(\tau; b) = H_y(\tau),$$

where  $H_y(\tau) \approx y(t(\tau))$  is an interpolating polynomial of degree  $g$  that satisfies  $g - 1$  solution values  $y_j$ , and whose derivative  $H'_y(\tau)$  satisfies one total derivative  $F$  from Definition 4.2; specifically for  $g$  distinct indices  $\nu \in \{1, \dots, w\}$ ,  $H_y(\tau_\nu) = y_\nu$ , and for one index  $s \in \{1, \dots, w\}$ ,  $H'_y(\tau_s) = F$ .

If the number of components  $m = 1$ , then both formulas reduce to the classical Adams ODE polynomials (3.3) and the classical BDF ODE polynomials (3.5).

**4.2. Additive polynomial block methods.** Block methods [38] are multivalued integrators that advance a set (or “block”) of points at each timestep. If we take  $s = 0$  in (3.8), then we obtain a polynomial block method (PBM) [14, 9, 11]. PBMs are simpler to derive compared to more general polynomial GLMs since all the ODE polynomials that determine the outputs are constructed using only input and output data. For this reason, PBMs were used to introduce both classical polynomial methods [14] and exponential polynomial methods [13]; in this paper we will use PBMs once more to introduce additive polynomial integrators.

An additive PBM depends on the parameters

$$\begin{aligned} q & \text{ number of inputs/outputs,} & \{z_j\}_{j=1}^q & \text{ nodes, } z_j \in \mathbb{C}, |z_j| \leq 1, \\ r & \text{ node radius, } r \geq 0, & \{b_j\}_{j=1}^q & \text{ expansion points,} \\ \alpha & \text{ extrapolation factor,} \end{aligned}$$

and can be written as

$$(4.8) \quad y_j^{[n+1]} = p_j(z_j + \alpha; b_j), \quad j = 1, \dots, q,$$

where each  $p_j(\tau; b)$  is a partitioned ODE polynomial built from the partitioned ODE

dataset

$$D(r, t_n) = \begin{cases} \text{inputs} : \left\{ \left( z_j, y_j^{[n]}, f_j^{\{1\}[n]}, \dots, f_j^{\{m\}[n]} \right) \right\}_{j=1}^q \\ \text{outputs} : \left\{ \left( z_j + \alpha, y_j^{[n+1]}, f_j^{\{1\}[n+1]}, \dots, f_j^{\{m\}[n+1]} \right) \right\}_{j=1}^q. \end{cases}$$

Any additive polynomial block method can be written in coefficient form as

$$(4.9) \quad \mathbf{y}^{[n+1]} = \mathbf{A}(\alpha)\mathbf{y}^{[n]} + r \sum_{k=1}^m \mathbf{B}^{\{k\}}(\alpha)\mathbf{f}^{\{k\}[n]} + r \sum_{k=1}^m \mathbf{C}^{\{k\}}(\alpha)\mathbf{f}^{\{k\}[n+1]}$$

where the matrices  $\mathbf{A}(\alpha)$ ,  $\mathbf{B}^{\{k\}}(\alpha)$ ,  $\mathbf{C}^{\{k\}}(\alpha) \in \mathbb{R}^{q \times q}$ , while the solution vectors and  $k$ th derivative component vectors are defined using  $\mathbf{y}^{[n]} = [y_1^{[n]}, \dots, y_q^{[n]}]^T$  and  $\mathbf{f}_j^{\{k\}[n]} = [f_1^{\{k\}[n]}, \dots, f_q^{\{k\}[n]}]^T$ .

Lastly, additive PBMs are just one example of the more general class of additive polynomial GLMs, described in the following remark.

*Remark 4.4 (Additive polynomial GLMs).* The formula for an additive polynomial method with  $s$  stages and  $q$  outputs is equivalent to (3.8) except that each  $p_j(\tau; b)$  is now a partitioned ODE polynomial constructed from a partitioned ODE datasets containing the method's input, output, and stage values. The family of additive polynomial GLMs is vast, therefore we cannot provide a detailed exploration of such methods in this work. However, in Section 5.2 we will see one example of an additive polynomial GLM that is constructed by composing multiple PBMs.

**4.3. Linear stability.** Linear stability analysis [28, IV.2] characterizes the behavior of a time integrator applied to the Dahlquist test problem  $y' = \lambda y$ , and is essential for determining which types of problems cause instabilities. To study the linear stability properties of an additive integrator, we use the partitioned Dahlquist equation [6, 37, 29]

$$(4.10) \quad y' = \sum_{j=1}^m \lambda_j y, \quad y(0) = y_0,$$

where  $\lambda_j y$  represents the  $j$ th component. The nonlinear problem (4.1) reduces to the partitioned Dahlquist equation if all  $f^{\{j\}}(t, y)$  are autonomous, diagonalizable linear operators that share the same eigenvectors.

When applied to (4.10), any additive polynomial integrator that accepts  $q$  inputs reduces to the matrix iteration

$$(4.11) \quad \mathbf{y}^{[n+1]} = \mathbf{M}(z_1, z_2, \dots, z_m, \alpha)\mathbf{y}^{[n]}$$

where  $\mathbf{y}_k^{[n]} = y_k^{[n]}$ ,  $k = 1, \dots, q$ ,  $\mathbf{M}: \mathbb{C}^m \times \mathbb{R}^+ \rightarrow \mathbb{C}^{q \times q}$ ,  $z_j = h\lambda_j$ , and  $h$  is the timestep. The stability region  $S$  is the subset of  $\mathbb{C}^m \times \mathbb{R}^+$  where  $\mathbf{M}(z_1, \dots, z_m, \alpha)$  is power bounded, so that

$$(4.12) \quad S = \left\{ z \in \mathbb{C}^m, \alpha \in \mathbb{R}^+ \mid \sup_{n \in \mathbb{N}} \|\mathbf{M}(z_1, \dots, z_m, \alpha)^n\| < \infty \right\}.$$

Therefore, the method is stable if the eigenvalues of  $\mathbf{M}(z_1, \dots, z_m, \alpha)$  lie inside the closed unit disk, and any eigenvalues of magnitude one are non-defective.

In Section 5 we will study the stability of additive polynomial integrators with  $m = 2$ . There are two important cases that we will discuss. First, if one selects the splitting (2.8), then  $z_1 = h \frac{\partial f}{\partial y}(y_n) = h(\lambda_1 + \lambda_2)$  and  $z_2 = 0$ . Therefore, the stability region of the additive integrator is equivalent to the stability region of the integrator used for the first component. For all the remaining splittings (2.4)-(2.6) it follows that  $z_2 \neq 0$  and the resulting stability region is five dimensional. To present these regions we overlay two-dimensional slices of the stability regions that are formed by fixing  $\alpha$  and  $z_1$  while allowing  $z_2$  to vary. Specifically, if we constrain  $z_1$  to the ray  $z_1 = re^{i\theta}$  then the corresponding stability region is

$$(4.13) \quad S_{r,\theta} = \{z_2 \in \mathbb{C} \mid R(re^{i\theta}, z_2) \leq 1\} \quad \text{where} \quad R(z_1, z_2) := \rho(\mathbf{M}(z_1, z_2, \alpha)),$$

and  $\rho(\cdot)$  denotes the spectral radius. The radius  $r$  determines the stiffness of the implicit component, and the angle  $\theta$  allows us to control the type of problem. In a PDE setting,  $\theta = \pi/2$  approximately represents a skew-symmetric advection discretization, while  $\theta = \pi$  approximately represents a symmetric positive-definite diffusion discretization. An intermediate value,  $\theta \in (\pi/2, \pi)$ , approximately represents a mix of advection and diffusion.

Since all real-valued discretizations of PDEs have spectrums that are symmetric about the imaginary axis, we consider the somewhat stricter stability region

$$(4.14) \quad \hat{S}_{r,\theta} = \{z_2 \in \mathbb{C} \mid \max(R(re^{i\theta}, z_2), R(re^{-i\theta}, z_2)) < 1\}.$$

To plot these stability regions in two dimensions we hold  $\alpha$  and  $\theta$  constant, and overlay several contours pertaining to different values of  $r$ . Lastly, we also consider the region

$$(4.15) \quad \hat{S}_\theta = \{z_2 \in \mathbb{C}, r \in \mathbb{R}^+ \mid \max(R(re^{i\theta}, z_2), R(re^{-i\theta}, z_2))\}$$

that contains all the  $z_2$  values that ensure stability for any  $z_1 = re^{i\omega}$  in the wedge consisting of  $r \geq 0$  and  $\theta \leq \omega \leq 2\pi - \theta$ .

### 5. Constructing IMEX polynomial integrators based on Radau IIA.

The additive polynomial framework enables the construction of additive PBMs for the general partitioned equation (4.1). However, in this introductory work we will focus on constructing IMEX methods for the simpler doubly partitioned equation (2.1) where  $f^{\{1\}}$  is treated implicitly and  $f^{\{2\}}$  is treated explicitly. In particular, we will introduce a family of arbitrary-order IMEX integrators that are based on the fully implicit Radau IIA methods described in Section 3.1.

To introduce an IMEX method with an implicit part that is equivalent to Radau IIA, we start by reusing the nodes (3.11) where we assume that  $q \geq 2$ . As in Section 3.1, we construct a PBM whose outputs are all computed using a single Adams ODE polynomial  $p(\tau; b)$  such that

$$(5.1) \quad y_j^{[n+1]} = p(z_j + \alpha; b_j), \quad j = 1, \dots, q.$$

Since we are considering an additive integrator for two component systems, the Adams polynomial is now doubly partitioned. To obtain an IMEX integrator, we must treat the first component implicitly and the second component explicitly, that is

$$(5.2) \quad p(\tau; b) = \underbrace{L_y(b) + \int_b^\tau L_f^{\{1\}}(\xi) d\xi}_{\text{implicit approx.}} + \underbrace{\int_b^\tau L_f^{\{2\}}(\xi) d\xi}_{\text{explicit approx.}}.$$

If we want an implicit component that is equivalent to Radau IIA, then we must select  $L_y(\tau)$ ,  $L_f^{\{1\}}(\tau)$ ,  $b$  and  $\alpha$  identically to what was done in Section 3.1, namely:

- $L_y(\tau)$  is the polynomial of degree  $q - 1$  that interpolates all  $q$  inputs, such that  $L_y(z_j) = y_j^{[n]}$ ,  $j = 1, \dots, q$ .
- $L_f^{\{1\}}(\tau)$  is the polynomial of degree  $q - 2$  that interpolates the last  $q - 1$  output component derivatives  $f_j^{\{1\}[n+1]}$  such that  $L_f^{\{1\}}(z_j + \alpha) = r f_j^{\{1\}[n+1]}$ ,  $j = 2, \dots, q$ .
- The extrapolation factor is  $\alpha = 2$  and the lower integration bound is  $b = 1$ .

To form the explicit approximation, we now make use of the input derivative components  $f_j^{\{2\}[n]}$ . We propose two different strategies for selecting  $L^{\{2\}}(\tau)$ :

1. Use only the derivative components at the input Radau nodes; let  $L_f^{\{2\}}(\tau)$  be a polynomial of order  $q - 2$  that satisfies

$$(5.3) \quad L_f^{\{2\}}(z_j) = r f_j^{\{2\}[n]} \quad j = 2, \dots, q.$$

2. Use all input derivative components; let  $L_f^{\{2\}}(\tau)$  be a polynomial of order  $q - 1$  that satisfies

$$(5.4) \quad L_f^{\{2\}}(z_j) = r f_j^{\{2\}[n]} \quad j = 1, \dots, q.$$

Both choices for  $L^{\{2\}}(\tau)$  lead to the multivalued IMEX method

$$(5.5) \quad y_j^{[n+1]} = y_q^{[n]} + \int_1^{z_j+2} L_f^{\{1\}}(s) + L_f^{\{2\}}(s) ds, \quad j = 1, \dots, q,$$

where the implicit component is equivalent to Radau IIA; notice that if  $f^{\{2\}}(t, y) = 0$ , then  $L^{\{2\}}(\tau) = 0$  and (5.5) is equivalent to (3.12). The order-of-accuracy of (5.5) is equal to the minimum order-of-accuracy of the implicit and explicit component. Because the implicit component is equivalent to Radau IIA with  $q - 1$  stages, its order-of-accuracy is  $2q - 3$ . Depending on whether we choose the polynomial (5.3) or (5.4) the explicit component respectively has an order of  $q - 1$  or  $q$ . Therefore, for all  $q > 2$ , the explicit component determines the overall accuracy and the higher-order polynomial is desirable. However, in Section 5.3 we will see that the higher-order polynomial also leads to inferior stability properties.

From here on, we will refer to the IMEX method with (5.3) as IMEX-Radau and the IMEX method with (5.4) as IMEX-Radau\*. In Figure 3 we present an illustration of the polynomials  $L_f^{\{1\}}(\tau)$  and  $L_f^{\{2\}}(\tau)$  for an IMEX-Radau method with  $q = 3$ , and below we also show the coefficients for the method:

$$(5.6) \quad \begin{aligned} y_1^{[n+1]} &= y_3^{[n]} \\ y_2^{[n+1]} &= y_3^{[n]} + \frac{5}{6} r f_2^{\{1\}[n+1]} - \frac{1}{6} r f_3^{\{1\}[n+1]} - \frac{1}{6} r f_2^{\{2\}[n]} + \frac{5}{6} r f_3^{\{2\}[n]} \\ y_3^{[n+1]} &= y_3^{[n]} + \frac{3}{2} r f_2^{\{1\}[n+1]} + \frac{1}{2} r f_3^{\{1\}[n+1]} - \frac{3}{2} r f_2^{\{2\}[n]} + \frac{7}{2} r f_3^{\{2\}[n]} \end{aligned}$$

Notice that if  $f^{\{2\}}(t, y) = 0$ , then (5.6) is equivalent to (3.13).

Any IMEX-Radau or IMEX-Radau\* method with  $q$  nodes can be written in the coefficient form

$$(5.7) \quad \mathbf{y}^{[n+1]} = \mathbf{A} \mathbf{y}^{[n]} + r \mathbf{B}^{\{1\}} \mathbf{f}^{\{1\}[n+1]} + r \mathbf{B}^{\{2\}} \mathbf{f}^{\{2\}[n]}$$

where  $\mathbf{A}$ ,  $\mathbf{B}^{\{1\}}$ ,  $\mathbf{B}^{\{2\}} \in \mathbb{R}^{q \times q}$ . In supplementary materials Section ?? we provide the coefficients for  $q = 2, 3, 4$ , along with a MATLAB script for initializing coefficients for

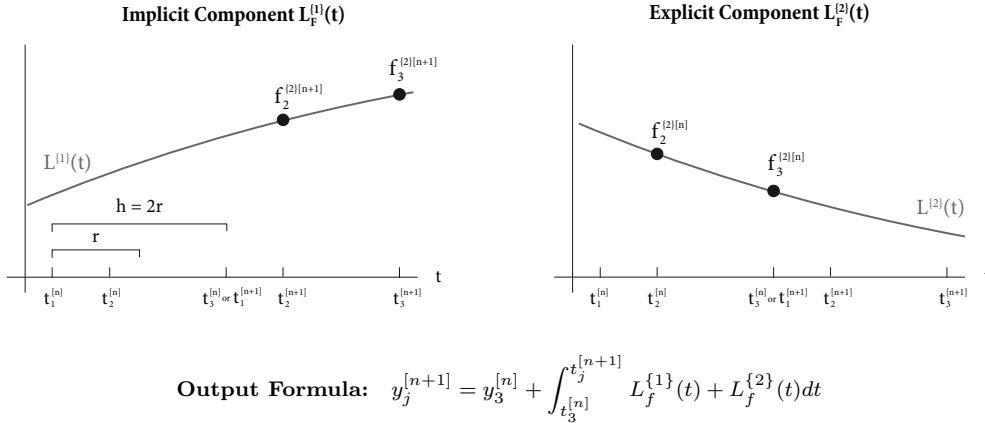


**Fig. 3:** An illustration depicting the polynomials in global time  $t$  that determine the outputs of the polynomial IMEX-Radau method (5.5) with  $q = 3$  and nodes  $\{z_j\} = \{-1, -1/3, 1\}$ . The nodes  $t_j^{[n]}$  are the nodes  $z_j$  in global coordinates at the  $n$ th timestep such that  $t_j^{[n]} = t_n + rz_j$ .

larger  $q$ . When  $q = 2$ , the IMEX-Radau method is equivalent to the IMEX-Euler method (2.3), while IMEX-Radau\* treats the the implicit component with backwards Euler and the explicit component with second-order Adams-Bashforth. For  $q > 2$ , the nonlinear implicit equations that arise in both IMEX-Radau methods (5.7) are analogous to those that arise in standard Radau IIA integration, with a modified right-hand side derived from the explicit component (i.e., linear and nonlinear solvers developed for fully implicit RK [18, 35, 25, 30, 36, 41, 40] naturally apply to IMEX-Radau).

Note that the method construction described here also applies to different node sets. For example, if we had selected Legendre nodes, then the implicit component would be equivalent to that of the fully implicit Gauss methods. However, Radau nodes have the advantage that they lead to an L-stable implicit component. Lastly, this method construction shares many similarities with the exponential PBM methods based on Legendre nodes from [13]. Loosely speaking, we have traded the exponential for a fully implicit approximation and switched from Legendre nodes to Radau nodes.

**5.1. A IMEX Radau iterator for obtaining initial conditions.** PBMs with  $q > 1$ , including (5.5), require multiple inputs at the first time-step. Though a one-step method can be used to compute these solution values, it may not always be possible to match the order of a starting method with that of the PBM. In [13] we proposed to use an iterator (a polynomial method with  $\alpha = 0$  described in Section 3.2) to compute the initial conditions of exponential PBMs. The iterator used a discrete exponential Picard iteration to improve the accuracy of an approximate solution. We can reuse the same idea in the context of additive integrators. In fact, it is always possible to construct a polynomial iterator that improves the accuracy of solution values relative to one or more highly accurate inputs [9, Ch. 6.2].

We can obtain a fully-implicit iterator by replacing  $\alpha = 2$  with  $\alpha = 0$  in (5.5) so that the upper integration bound is just  $z_j$ . However this iterator steps backwards in time, which introduces additional complications. By modifying the method construction so that  $b_j = -1$ , we can avoid integrating backwards in time. This leads to the

iterator

$$(5.8) \quad y_j^{[n+1]} = y_1^{[n]} + \int_{-1}^{z_j} L_f^{\{1\}}(s) + L_f^{\{2\}}(s) ds, \quad j = 1, \dots, q,$$

that uses the Radau IIA coefficients for both the implicit and explicit parts. For example, when  $q = 3$ , we obtain the method

$$(5.9) \quad \begin{aligned} y_1^{[n+1]} &= y_1^{[n]} \\ y_2^{[n+1]} &= y_1^{[n]} + \frac{5}{6} r f_2^{\{1\}[n+1]} - \frac{1}{6} r f_3^{\{1\}[n+1]} + \frac{5}{6} r f_2^{\{2\}[n]} - \frac{1}{6} r f_3^{\{2\}[n]} \\ y_3^{[n+1]} &= y_1^{[n]} + \frac{3}{2} r f_2^{\{1\}[n+1]} + \frac{1}{2} r f_3^{\{1\}[n+1]} + \frac{3}{2} r f_2^{\{2\}[n]} + \frac{1}{2} r f_3^{\{2\}[n]}. \end{aligned}$$

Note that both the implicit and explicit coefficients in the iterator (5.9) are identical to the implicit coefficients in the propagator (5.6). If  $y_1^{[n]}$  is of order  $2q - 3$  or higher, then every application of the iterator (5.8) will improve the order-of-accuracy of all other solution values by one, up to a maximum order of  $2q - 3$ . Moreover, when a repeatedly applied iteration converges, then the PBM outputs are equivalent to the output and stage values of a fully-implicit Radau IIA method with  $q - 1$  stages.

We can therefore use (5.8) to compute initial conditions in the following way. We first consider an iterator with quadrature points on the interval  $[0, 2]$ , instead of  $[-1, 1]$ . The method has identical coefficients, however the first input node at  $z_1 = 0$  is now located at  $t = t_0$  where the initial condition for (1.1) is provided (i.e.  $y_1^{[0]} = y(rz_1 + t_0) = y_0$ ). Next we obtain a zeroth-order estimate for the solution at all the input nodes by temporarily assuming a constant solution such that  $y_j^{[n]} = y_0$ . Last, we repeatedly apply the iterator to improve the accuracy of the zeroth-order estimate. This procedure provides an accurate initial solution at the times  $t = t_0 + rz_j$  for  $j = 1, \dots, q$ , and can be written abstractly as

$$(5.10) \quad \mathbf{y}^{[0]} = M^\kappa(\mathbf{c}), \quad \mathbf{c}_j = y_0, \quad j = 1, \dots, q,$$

where  $\mathbf{c}$  is the initial zeroth-order approximation, and  $M^\kappa(\mathbf{c})$  is the iterator method applied the  $\kappa$  times to initial condition  $\mathbf{c}$  such that  $M^\kappa(c) = M(M(\dots(M(c))))$ . For an IMEX-Radau or IMEX-Radau\* method, the iterator should be respectively applied a minimum of  $\kappa = q - 1$  and  $\kappa = q$  times at the first step to match the order of the explicit component.

**5.2. Composite IMEX Radau methods.** The method (5.5) where  $L^{\{2\}}(\tau)$  is selected using (5.3) pairs a fully implicit integrator of order  $2q - 3$  with an explicit integrator of order  $q - 1$ . Therefore, the combined order is limited to  $q - 1$ . Using (5.4) improves the order by one, however the imbalance in accuracy between the implicit and explicit component remains. One strategy for increasing accuracy further, is to use a composite method that first advances the timestep with the propagator (5.6) and then corrects the output of the propagator  $\kappa$  times using the iterator (5.9). This idea of composite PBMs was introduced in [13] for exponential integrators and shares many similarities with spectral deferred correction methods [24, 34, 10]. In the following sections we show how the same idea leads to composite additive integrators with improved stability and accuracy properties.

The composite method can be written abstractly as

$$(5.11) \quad \mathbf{y}^{[n+1]} = M^\kappa(P(\mathbf{y}^{[n]})),$$



when  $P(\cdot)$  denotes the propagator (5.5) where  $L_f^{\{2\}}$  is selected using (5.3) or (5.4), and  $M^\kappa(\cdot)$  denotes  $\kappa$  applications of the iterator (5.8). We will refer to this composite method as IMEX-Radau( $q, \kappa$ ) if  $P$  is (5.3) and IMEX-Radau\*( $q, \kappa$ ) if  $P$  is (5.4);  $q$  is the number of nodes and  $\kappa$  is the number of iterator applications. Since each application of the iterator improves the accuracy order by one, the associated order-of-accuracy for these methods is

(5.12)

$$\text{IMEX-Radau}(q, \kappa) \quad \min(2q - 3, q - 1 + \kappa)$$

(5.13)

$$\text{IMEX-Radau}^*(q, \kappa) \quad \min(2q - 3, q + \kappa)$$

Last, it is important to note that when using iterative methods to solve the implicit equations (as in numerical PDEs), the implicit solve for the iterator will typically be significantly faster than the propagator, due to a very good initial guess. That is, rather than advance a set of solutions forward in time by  $h$  like a propagator, an iterator simply increase the accuracy of the *current* solutions by one.

**5.3. Linear stability.** If an IMEX-Radau method is implemented using the splitting (2.4), then we obtain excellent linear stability properties since the class of Radau IIA methods are all L-stable [28, IV.5]. However, to analyze the stability properties for more general splittings, we consider the stability regions  $\hat{S}_{r,\theta}$  defined in (4.14).

In Figure 4 we plot several stability regions for the composite method IMEX-Radau\*( $4, \kappa$ ) from (5.11) with  $\kappa = 0, 1, 2$ . When  $\kappa = 0$  the IMEX-Radau\*( $4, 0$ ) method is equivalent to the IMEX-Radau\* method (5.5) with  $q = 4$ . We consider stability regions  $\hat{S}_{r,\theta}$  for  $\theta$  values of  $0, \frac{3\pi}{2}$ , and  $\frac{\pi}{2}$  which respectively approximate an implicit linear component with diffusion, a mix of diffusion and oscillation, and pure oscillation.

The stability regions for IMEX-Radau\* are largest for the diffusive case with  $\theta = 0$  and smallest for the oscillatory case with  $\theta = \pi/2$ . For each of the three  $\theta$  values, the IMEX-Radau\*( $4, \kappa$ ) stability regions always enclose the imaginary axis. Despite the fact that IMEX-Radau\* is equipped with a fully implicit propagator, the stability regions grow slowly in  $r$  and are very small when  $\theta = \frac{\pi}{2}$ . However, even a single application of the iterator leads to significantly larger linear stability regions for all  $\theta$  values. Lastly, in supplemental materials Figure ?? we also show the equivalent stability regions for the composite IMEX-Radau method; overall we see that using a lower-order polynomial approximation for the explicit component leads to improved stability.

**6. Numerical Experiments.** We investigate the efficiency of IMEX-Radau and IMEX-Radau\* methods by conducting three types of numerical experiments. First, we study the performance of the integrators on PDEs with periodic domains where inverting the implicit component is trivial. Then, we compare both method families on a finite-element discretization of a non-periodic problem, where solving the fully implicit system requires special care [25, 30, 36, 41, 40]. Lastly, we numerically investigate order reduction on the singularly perturbed Van der Pol equation.

For certain spatial discretizations, such as spectral methods, and/or solvers that are difficult to parallelize, the IMEX-Radau methods allow for certain types of parallelization that are not feasible using existing IMEX-RK methods. For example, when considering periodic domains with Fourier discretizations, the implicit component is trivial to invert, and the majority of the cost is due to the nonlinear function evaluations. In Subsection 6.1 we demonstrate how parallelization of nonlinear function

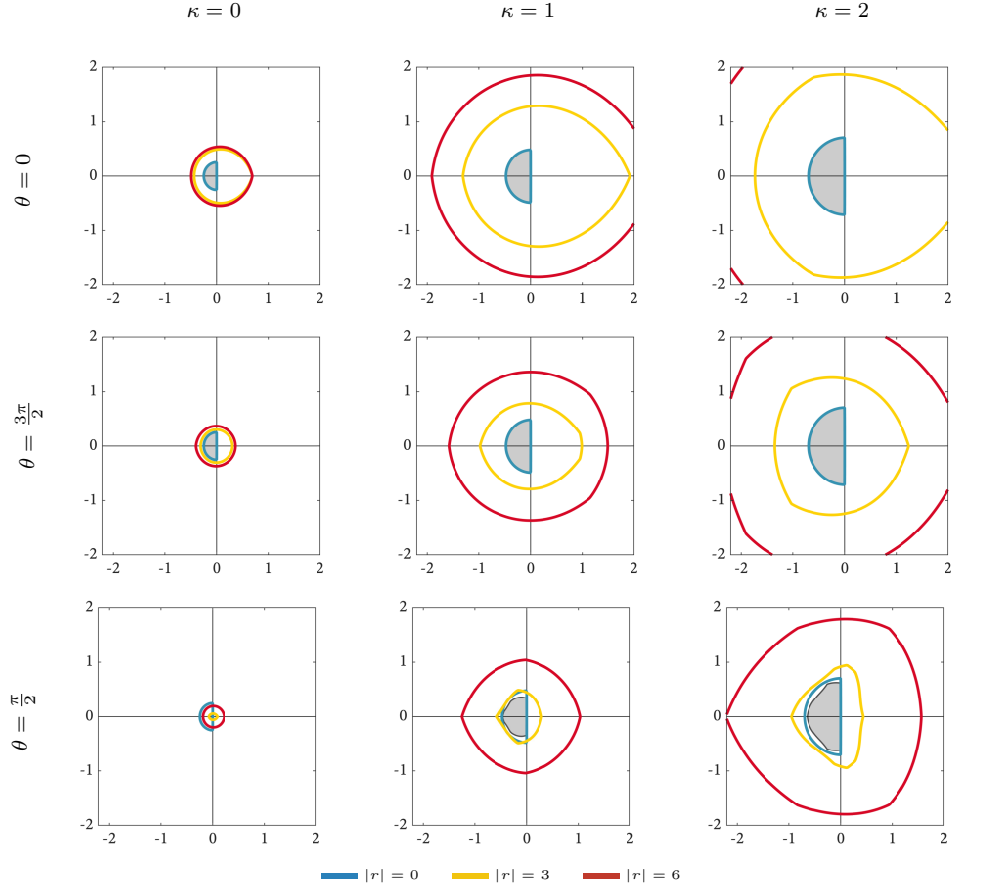


**Fig. 4:** Stability regions for IMEX-Radau\*( $q = 4, \kappa$ ). Each colored contour represents a different stability region  $R_{r,\theta}$  defined in (4.14). The gray region is the stability region  $R_\theta$  described in (4.15).

evaluations can be applied to obtain highly accurate solutions in significantly less time. More generally, there are situations such as when solver performance degrades in parallel, or when finite element construction and nonlinear function evaluations can be very expensive, where the additional parallelization provided by these IMEX-Radau can be exploited.

Conversely, with finite element discretizations and scalable solvers, spatial parallelism is often very effective. In Subsection 6.3 we investigate the efficiency of IMEX-Radau methods with traditional spatial parallelism on a problem where function evaluations are relatively cheap and time-parallelism is not needed.

**6.1. PDEs with periodic boundary conditions.** In this experiment we evaluate the accuracy and efficiency of composite IMEX-Radau\* methods (5.11) on the dispersive Korteweg-De Vries equation with periodic boundary conditions. For comparison we also include results for IMEX-RK integrators of orders one to four; specifically the (1,1,1) and (2,3,2) methods from [Sec. 2.1, 2.5][5], and the ARK3(2)4L[2]SA and ARK4(3)6L[2]SA from [31]. The numerical experiment is identical to one found in [13, 10] and is only briefly described below:

1. The **Korteweg-de Vries** (KDV) equation from [44, 10, 13]

$$\frac{\partial u}{\partial t} = - \left[ \delta \frac{\partial^3 u}{\partial x^3} + \frac{1}{2} \frac{\partial}{\partial x} (u^2) \right] \quad \begin{array}{l} u(x, t = 0) = \cos(\pi x), \\ x \in [0, 2], \end{array}$$

where  $\delta = 0.022$ . This equation is integrated to time  $t = 3.6/\pi$  using a 512 point Fourier spectral discretization.

**6.1.1. Implementation details.** We solve the KDV equation in Fourier space so that the initial value problem has the form  $\mathbf{y}' = \mathbf{L}\mathbf{y} + N(t, \mathbf{y})$  where  $\mathbf{L}$  is an  $N \times N$  diagonal matrix that includes the discretized linear differential operator. For dealiasing we apply the standard 3/2 rule that zeros out the top third of the spectrum. Since  $\mathbf{L}$  is diagonal, the implicit solve for a fully-implicit propagator or iterator (5.7) amounts to inverting  $N$  decoupled  $q \times q$  systems of the form  $(\mathbf{I} - r\mathbf{L}_{kk}\mathbf{B}^{\{2\}})\mathbf{x} = \mathbf{b}$  for  $k = 1, \dots, N$ . To save computational time the matrix inverses for Radau propagators and iterators are precomputed and stored at the first timestep. In this way, an implicit solve can be done using  $N$ ,  $q \times q$  matrix multiplications. Since this operation is cheap, the dominant computational cost for all integrators on these problems is the nonlinear function evaluations.

IMEX-Radau integrators benefit from time parallelism since the nonlinear function evaluations and output computations can be computed simultaneously. To quantify the benefits of parallelism, we created both serial Fortran implementations of the integrators and parallel Fortran implementations using OpenMP. An IMEX-Radau method with  $q$  nodes requires  $q$  independent function evaluations that can be computed simultaneously using  $q$  shared or distributed memory processes / threads. In contrast an IMEX-RK method requires sequential evaluation of the nonlinear term at each stage, therefore this type of parallelization is not possible. However, all methods can benefit from spatial parallelization where the FFT evaluations are computed using multiple threads. For the purposes of this experiment we will only investigate time parallelism and compute all FFT evaluations using one thread.

Our Fortran code can be found in [12], and all the timing results presented in this subsection were produced on a 14 core, 2.0 Ghz Intel Xeon E5-2683 v3 with hyper-threading enabled.

**6.1.2. Results and discussion.** In Figure 5 we present results for the KDV equation solved using composite IMEX-Radau $^*(q, 2)$  methods with  $q = 2, 3, 4, 5$ . We select  $\kappa = 2$  since the linear stability regions from Figure 4 revealed that IMEX-Radau $^*(q, 0)$ , have comparatively poor stability for non-diffusive equations. Overall the IMEX-Radau $^*(q, 2)$  integrators performed excellent, with the serial, seventh-order IMEX-Radau $^*(5, 2)$  outperforming all the other methods for any desired accuracy. When using OpenMP parallelism with five threads, the IMEX-Radau $^*(5, 2)$  method was even more efficient, and capable of obtaining the solution with a relative error of  $10^{-2}$  approximately two times faster than any RK method. For more accurate solutions with errors below  $10^{-4}$ , the difference was even more significant and IMEX-Radau $^*(5, 2)$  was able to obtain the solution approximately thirty times faster than IMEX-RK4. For lower-order methods, the third-order IMEX-Radau $^*(3, 2)$  method exhibited increased fourth-order convergence throughout most of the stepsize range. This enabled the method to be more efficient than the IMEX-RK4 method, despite only requiring the storage of three solution vectors instead of the five needed by the RK method. Lastly, if very inaccurate solutions are sufficient, then the IMEX-Radau $^*(2, 1)$  method was both more efficient and more stable than the IMEX-RK1 (or equivalently IMEX-Radau(2, 0)) method.

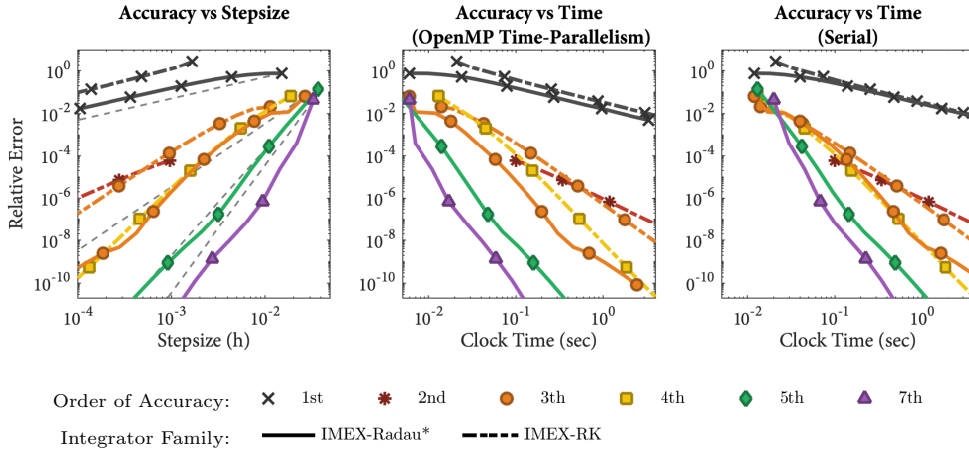


**Fig. 5:** Accuracy and precision diagrams comparing composite IMEX-Radau $^*(q, 2)$  with  $q = 2, 3, 4, 5$  to IMEX-RK on the KDV equation. All curves start at the first stable timestep. The parallel and serial time plots respectively show run times for composite IMEX-Radau $^*(q, 2)$  methods with and without OpenMP parallelization. The dashed lines of increasing slope in the accuracy plot respectively correspond to first, third, fifth, and seventh order convergence which are the expected orders of convergence (5.13) for IMEX-Radau $^*$ .

**6.2. Numerically investigating order reduction.** In this experiment we numerically investigate order reduction for the composite IMEX-Radau method (5.11) by solving the Van der Pol equation [28, p. 403]

$$(6.1) \quad \begin{aligned} y_1' &= y_2 & y_1(0) &= 2 \\ y_2' &= \frac{(1 - y_1^2)y_2 - y_1}{\epsilon} & y_2(0) &= -\frac{2}{3} + \frac{10}{81}\epsilon - \frac{292}{2187}\epsilon^2 - \frac{1814}{19683}\epsilon^3 \end{aligned}$$

integrated to time  $t = 0.5$ . We consider  $\epsilon$  values ranging from  $\epsilon = 1$  to  $\epsilon = 10^{-8}$ . When the stiffness parameter  $\epsilon$  is small, this equation is known to cause order-reduction for IMEX-RK methods [5, 7, 31, 33, 29, 32].

We integrate the Van der Pol equation using composite IMEX-Radau method (5.11) where the propagator uses (5.3),  $q \in \{3, 4, 5\}$  and  $\kappa \in \{0, 1, 2\}$ . The equation right-hand-side is split in two different ways. The first splitting will be called semi-implicit since it treats the first component explicitly and the second component implicitly; this same splitting was used in [29, 5, 7, 33, 31, 32]. We also consider the semi-linear splitting (2.8) where  $J_n$  is the exact Jacobian of the right-hand-side at the  $n$ th timestep.

To validate IMEX-Radau( $q, \kappa$ ) methods, we estimate their convergence rates as a function of  $\epsilon$ . The procedure we use to approximate convergence rates is based on the one proposed in [32]. Specifically, we solve (6.1) using 30 logarithmically spaced stepsizes ranging from  $h = 0.25$  to  $h = 10^{-4}$  and then compute a linear least-squares fit of  $\log(\text{error})$  versus  $\log(\text{stepsize})$ . Error is measured relative to a reference solution that was computed using the MATLAB ode15s integrator.

In Figure 6 we show convergence rate plots and convergence diagrams for the IMEX-Radau( $q, \kappa$ ) method with each splitting. There are several important points regarding the results:

- IMEX-Radau methods are stable across the full range of stepsizes for both splittings. The linearly-implicit splitting does not require a nonlinear solve at each step, leading to improved computational efficiency. In contrast, all the IMEX-RK methods we tested from [32, 31] required substantially smaller timesteps to remain stable with the linearly-implicit splitting (See Figure ??).
- For small  $\epsilon$ , each application of the iterator raises the order of convergence by approximately one. For  $\epsilon$  between  $10^{-2}$  and  $10^{-4}$  we see a decreased convergence rate for Radau( $q,2$ ) methods using the semi-implicit splitting. However the extra iteration improves accuracy significantly. For example, from the convergence diagram for  $\epsilon = 10^{-3}$ , we see that IMEX-Radau( $q,3$ ) is always more accurate than IMEX-Radau( $q,2$ ), despite its slower convergence rate.
- The estimated convergence rates are consistently smaller than the expected order-of-accuracy (5.12). However, the reduced convergence order is a symptom of minor order reduction at coarse stepsizes  $h \geq .1$  (less than 5 total timesteps). By including this data in our least squares fits we see lower overall convergence rates. If we only consider  $h < .1$ , then we would observe expected convergence (for example, we can see that the convergence curves for  $h < .1$  match the dashed convergence-order lines in the diagrams in Figure ??).
- The convergence rates for Radau( $3,\kappa$ ) with a linearly-implicit splitting are unusually high for  $\kappa = 2$ . This is due to rapid convergence at coarse timesteps that leads to higher than expected overall convergence. Nevertheless, for sufficiently small stepsizes, the convergence limits to third-order (e.g. see the convergence diagram for  $\epsilon = 10^{-3}$ ). Interestingly, as  $\epsilon$  decreases, the region of rapid convergence increases, and for any  $\epsilon < 10^{-5}$  we would have to solve the equation in high precision arithmetic to see the proper convergence order.

**6.3. DG advection-diffusion.** Here we consider the time-dependent advection-diffusion equation

$$(6.2) \quad u_t + \nabla \cdot (\beta u - \varepsilon \nabla u) = f,$$

where  $\beta(x, y) := (1, 1)^T$  is the velocity field and  $\varepsilon$  the diffusion coefficient. We choose the forcing function  $f(x, y, t)$  such that the analytical solution is given by  $u_*(x, y, t) = \sin(2\pi x(1-y)(1+2t)) \sin(2\pi y(1-x)(1+2t))$ ; this allows us to measure the  $\ell^2$ -error of the discrete solution.

We discretize (6.2) in space using discontinuous Galerkin finite elements over the spatial domain  $\Omega = [0, 1] \times [0, 1]$ . Dirichlet boundary conditions are weakly enforced on  $\partial\Omega$ , advection terms are upwinded [20], and diffusion terms are treated with the symmetric interior penalty method [3, 4]. Let  $V_h$  be the DG finite element space consisting of piecewise polynomials of degree  $p$  defined locally on elements of the spatial mesh  $\mathcal{T}$ . The resulting finite element problem is to find  $u_h \in V_h$  such that, for all  $v_h \in V_h$ ,

$$\begin{aligned} & \int_{\Omega} \partial_t(u_h)v_h \, dx - \int_{\Omega} u_h \beta \cdot \nabla_h v_h \, dx + \int_{\Gamma} \widehat{u}_h \beta \cdot \llbracket v_h \rrbracket \, ds + \int_{\Omega} \nabla_h u_h \cdot \nabla_h v_h \, dx \\ & - \int_{\Gamma} \{\nabla_h u_h\} \cdot \llbracket v_h \rrbracket \, ds - \int_{\Gamma} \{\nabla_h v_h\} \cdot \llbracket u_h \rrbracket \, ds + \int_{\Gamma} \sigma \llbracket u_h \rrbracket \cdot \llbracket v_h \rrbracket \, ds = \int_{\Omega} f v_h \, dx, \end{aligned}$$

where  $\nabla_h$  is the broken gradient,  $\Gamma$  denotes the skeleton of the mesh,  $\{\cdot\}$  and  $\llbracket \cdot \rrbracket$  denote the average and jump operators, respectively, and  $\widehat{u}_h$  is used to denote the upwind numerical flux. The parameter  $\sigma$  is the *interior penalty parameter*, important for a stable discretization [4], which we set to  $\sigma = (p+1)^2/h$ .

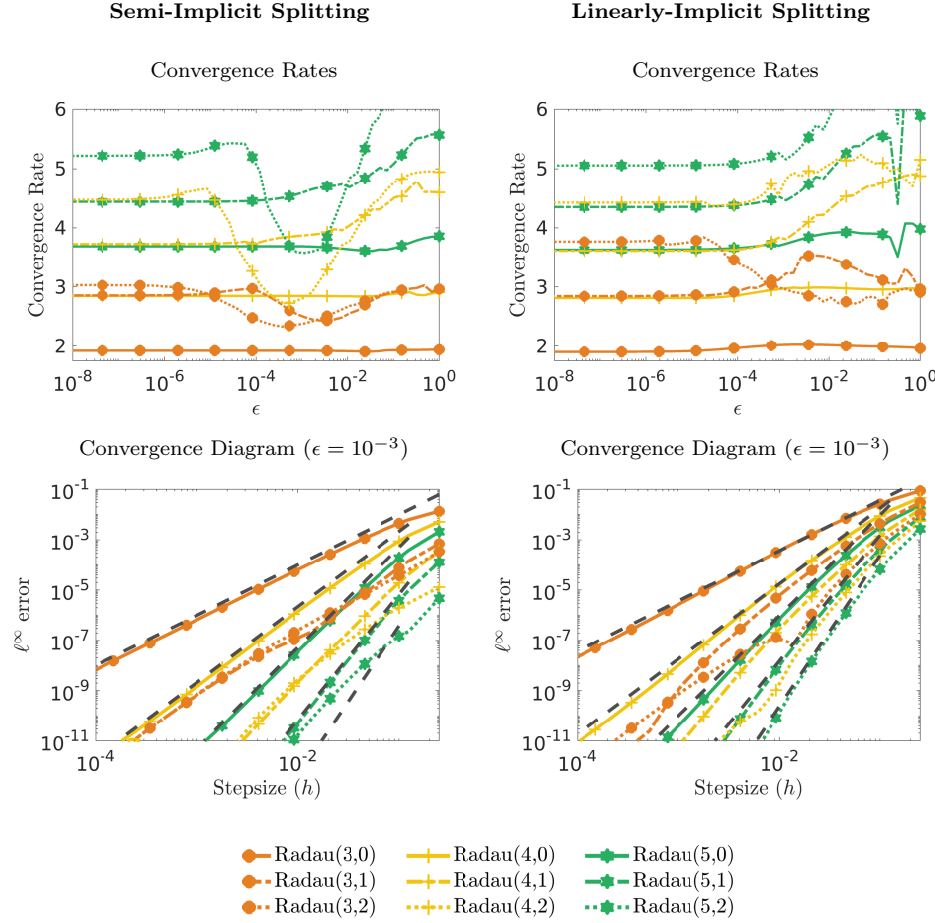


**Fig. 6:** Approximate overall convergence rates for the Van der Pol equation (6.1) as a function of  $\epsilon$  (top row), and two example convergence diagrams (bottom row). The left column contains results for the semi-implicit splitting while the right column show results for the linearly-implicit splitting. Lastly, the dashed lines in the bottom plots correspond to convergence orders of 3 through 6.

The discretization is implemented in the MFEM finite element library [2], and we take a standard advection-diffusion splitting of treating the advection explicitly and the diffusion and source term implicitly. Classical algebraic multigrid (AMG) in the *hypr*e library is used to solve the implicit diffusion equations. For the Radau schemes, we must solve an implicit system analogous to that which arises in fully implicit Runge Kutta methods. We wrap the AMG solver already mentioned with the block preconditioning for fully implicit Runge Kutta methods developed in [41, 40] to solve the Radau stage equations. We use 4th-order elements in space, with mesh spacing  $h_x \approx 0.0078$  leading to expected spatial accuracy  $\sim \mathcal{O}(10^{-9})$  and solve the implicit equations to  $10^{-12}$  relative residual to ensure  $\ell^2$ -error is not affected by an inexact implicit solve. All simulations are run to final (simulation) time  $t_f = 2$  on 4 dual socket Intel Xeon Gold 6152 22-core processors (i.e., 44 cores/node) with 120 total MPI processes.

**6.3.1. Runge Kutta Stability.** We first point out that stability of IMEX integration schemes for this fairly standard discretization is not trivial. As an example, we consider the two variations in first-order IMEX-Runge Kutta presented in [5], the RK(1,1,1) and RK(1,2,1) schemes. To understand stability, we note that a necessary condition is having the eigenvalues of the propagation operator bounded  $< 1$  in magnitude. Thus, we consider mesh spacing  $dx \approx 0.03$  and directly construct the propagation operators for the RK(1,1,1)- and RK(1,2,1)-schemes. Letting  $\epsilon = 1$  and  $h = 0.004876$  be the (numerically determined) forward Euler advective stability limit, eigenvalues for the two propagation operators are shown in Figure 7. Note that for this moderately small time step size, RK(1,2,1) is very unstable; numerical tests confirm this in practice, with the solution rapidly growing by orders of magnitude.

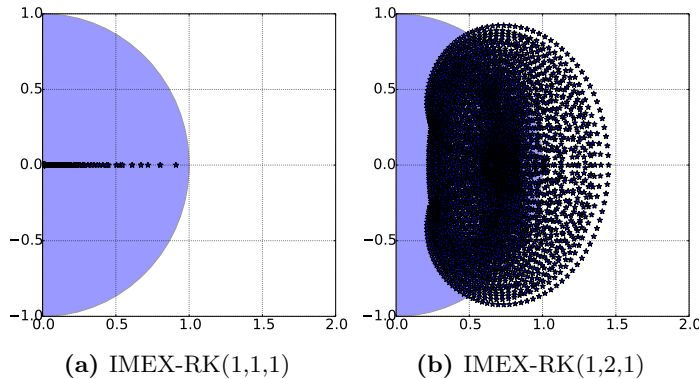


**Fig. 7:** Eigenvalues of propagation operator for two first-order IMEX-RK schemes from [5], with time-step  $h = 0.004876$  given by the advective stability limit. The unit circle is shaded; eigenvalues must be inside of shaded region for stable time propagation.

In fact, many of the IMEX-RK schemes proposed in [5] suffer from similar instabilities with this problem and discretization. The *only* schemes from [5] that have demonstrated reasonable stability here are schemes in which *both* the implicit and explicit method are stiffly accurate. Moving forward, we only consider these schemes, namely RK(1,1,1), RK(2,2,2), and RK(4,4,3) in the notation of [5]. In addition, we consider ESDIRK ARK3(2)4L[2]SA from [31], which we abbreviate ARK(4,3), and demonstrates stability for sufficiently small  $h$ .

**6.3.2. IMEX-Radau.** Here we compare the new IMEX-Radau\* methods with standard IMEX-RK up to third-order from [5, 31]. We consider IMEX-Radau\* because for  $q \lesssim 5$ , practice has indicated they consistently offer improved accuracy compared to IMEX-Radau methods, with only a marginal loss in stability. Figure 8 compares RK(1,1,1), RK(2,2,2), RK(4,4,3) [5], and ARK(4,3) [31], with IMEX-Radau\*( $q, \kappa$ ), for  $q \in \{2, 3, 4\}$  and  $\kappa \in \{0, 1, 2\}$ . Plots present solution accuracy with respect to time-step size,  $h$ , and total wallclock time to solution with respect to accuracy, for two different diffusion coefficients.

Notice that for both  $\epsilon \in \{0.1, 10\}$ , the IMEX-Radau methods are the most efficient in terms of error as a function of runtime to solution for accuracy  $\lesssim 10^{-3}$ . Moreover, for  $\epsilon = 0.1$  and  $\epsilon = 10$ , the IMEX-Radau\* methods obtain  $\sim 10^{-5}$  accuracy respectively  $\approx 16\times$  and  $\approx 16\times$  faster than the best IMEX-RK method, RK(4,4,3). For highly accurate iterations, IMEX-Radau\* are particularly beneficial, obtaining as many as 4 – 5 orders of magnitude smaller error than the best IMEX-RK meth-

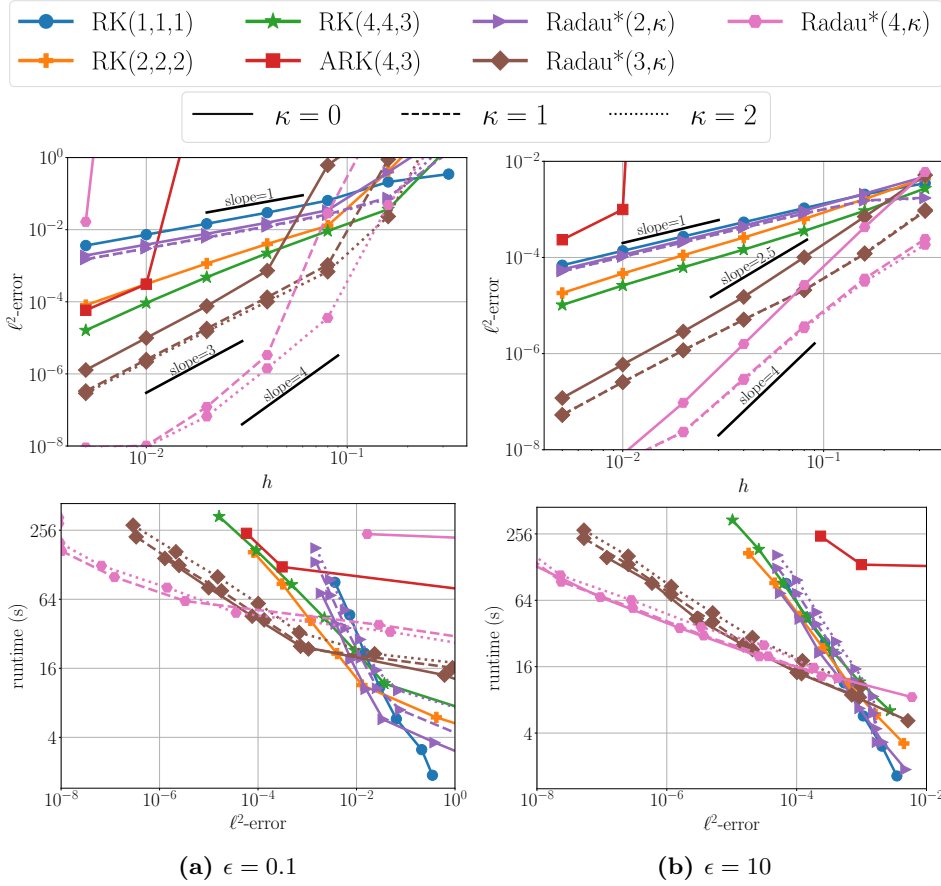


**Fig. 8:**  $\ell^2$ -accuracy as a function of  $h$  and wallclock time to solution.

ods, using the *same* computational runtime (including state-of-the art parallel linear solvers used for all methods).

In terms of order of convergence, we see that the IMEX-Radau\* methods observe their expected order of accuracy, or close, while 3rd-order IMEX-RK methods, ARK(4,3) and RK(4,4,3), suffer from order reduction, particularly for  $\epsilon = 10$ . We also point out that IMEX-Radau\*(2, $\kappa$ ) provides a simple improvement over standard IMEX-Euler, coupling backward Euler with a 2nd-order Adams-Bashforth explicit integrator, yielding a decrease in error of  $\approx 50\%$  for  $\epsilon = 0.1$  over standard IMEX-Euler.

In terms of accuracy as a function of wallclock time, the iterators are in some sense a wash, that is, applying one or two applications of an iterator tends to decrease the error roughly proportional with the cost of its application. The one caveat is that the iterators also provide improved stability. This is evident for  $\epsilon = 0.1$  and IMEX-Radau\*(4, $\kappa$ ), where the method largely diverges for  $\kappa = 0$  (except at the smallest  $h$  considered,  $h = 0.005$ ). However, applying one or two applications of the iterator then yields a stable, high-order method. Adaptive application of iterators will be a topic of future work.

To highlight the stability gains provided by iterators, consider  $\epsilon = 0.01$  and  $h = 0.01$ . Results for the *only* IMEX-RK methods that did not diverge are shown in Table 1, along with a selection of IMEX-Radau and IMEX-Radau\* methods that converge, typically with the application of one or more application of the iterator



to provide stability (for a given method, results are shown for the *lowest* number of iterators required for stability). Note, the one exception is IMEX-Radau\*(2,0), which again provides improved accuracy over IMEX-Euler, at a relatively trivial cost, and IMEX-Radau(2,1), which improves the accuracy of IMEX-Euler via the application of an iterator. Note that the IMEX-Radau\* methods again provide several orders of magnitude smaller error than RK(4,4,3), for a comparable wallclock time.

	RK(1,1,1)	Radau*(2,0)	Radau(2,1)	
$\ell^2$ -error	0.018	0.009	0.009	
runtime (s)	35	37	71	
	RK(4,4,3)	Radau(3,1)	Radau*(3,2)	Radau*(4,2)
$\ell^2$ -error	$7.4 \cdot 10^{-5}$	$2.1 \cdot 10^{-5}$	$2.6 \cdot 10^{-6}$	$2.9 \cdot 10^{-8}$
runtime (s)	165	122	151	184

**Table 1:**  $\ell^2$ -error and runtime in seconds for various integration schemes with  $\epsilon = 0.01$  and  $h = 0.01$ .

**7. Summary and Conclusion.** In the first half of this paper we introduced a general framework for constructing multivalued or one-step additive polynomial time integrators with any degree of implicitness. By utilizing interpolating polynomials, the framework enables the derivation of high-order methods without requiring the solution of nonlinear order conditions (even if the underlying equation has an arbitrary number of additive partitions). Moreover, by selecting high-order ODE polynomials, one trivially achieves high stage order that prevents order reduction on stiff problems. Lastly, the framework also naturally includes iterators that can be used to compute initial conditions and to construct composite PBMs with improved stability and accuracy properties.

The second-half of this paper focused exclusively on fully-implicit IMEX methods that utilize Adams ODE polynomials. Specifically we introduced a new class of IMEX-Radau integrators, which use a Radau IIA fully implicit component coupled with a parallel block method for the explicit component. In Section 6 we demonstrated the significant potential of these integrators in practice. In each of our experiments, IMEX-Radau methods consistently yielded the most accurate solution compared with other methods from [5, 31]. Moreover, thanks to recent developments in solvers for fully implicit Runge-Kutta methods [41, 40], they were also the fastest methods (in terms of total runtime) to obtain a given accuracy. Furthermore, by using iterators, the composite IMEX-Radau methods offer a simple way to develop very high-order IMEX integrators with low storage cost.

Thus far, we have only introduced one class of additive polynomial integrators. In part two of this work we will introduce new families of diagonally implicit IMEX-Polynomial integrators that are based on the BDF ODE polynomials. In addition, we point out that Radau and other fully implicit Runge-Kutta methods offer a number of unique advantages and properties that cannot be obtained with other classes of integrators. Future work will study the potential of IMEX-Radau and related integrators on topics such as differential algebraic equations and conservation of invariants which fully implicit Runge-Kutta methods are uniquely suited for.

**Acknowledgements.** Los Alamos National Laboratory report number LA-UR-21-28709.

## REFERENCES

- [1] G. AKRIVIS, O. KARAKASHIAN, AND F. KARAKATSANI, *Linearly implicit methods for nonlinear evolution equations*, *Numerische Mathematik*, 94 (2003), pp. 403–418.
- [2] R. ANDERSON, J. ANDREJ, A. BARKER, J. BRAMWELL, J.-S. CAMIER, J. CERVENY, V. DOBREV, Y. DUDOUIT, A. FISHER, T. KOLEV, W. PAZNER, M. STOWELL, V. TOMOV, J. DAHM, D. MEDINA, AND S. ZAMPINI, *MFEM: a modular finite element methods library*, *Computers & Mathematics with Applications*, (2020), <https://doi.org/10.1016/j.camwa.2020.06.009>.
- [3] D. N. ARNOLD, *An interior penalty finite element method with discontinuous elements*, *SIAM Journal on Numerical Analysis*, 19 (1982), pp. 742–760, <https://doi.org/10.1137/0719052>.
- [4] D. N. ARNOLD, F. BREZZI, B. COCKBURN, AND L. D. MARINI, *Unified analysis of discontinuous Galerkin methods for elliptic problems*, *SIAM Journal on Numerical Analysis*, 39 (2002), pp. 1749–1779, <https://doi.org/10.1137/S0036142901384162>.
- [5] U. M. ASCHER, S. J. RUUTH, AND R. J. SPITERI, *Implicit-explicit runge-kutta methods for time-dependent partial differential equations*, *Applied Numerical Mathematics*, 25 (1997), pp. 151–167.
- [6] U. M. ASCHER, S. J. RUUTH, AND B. T. WETTON, *Implicit-explicit methods for time-dependent partial differential equations*, *SIAM Journal on Numerical Analysis*, 32 (1995), pp. 797–823.
- [7] S. BOSCARINO, *Error analysis of imex runge-kutta methods derived from differential-algebraic systems*, *SIAM Journal on Numerical Analysis*, 45 (2007), pp. 1600–1621.
- [8] J. C. BUTCHER AND N. GOODWIN, *Numerical methods for ordinary differential equations*, vol. 2, Wiley Online Library, 2016.
- [9] T. BUVOLI, *Polynomial-Based Methods for Time-Integration*, PhD thesis, University of Washington, 2018.
- [10] T. BUVOLI, *A class of exponential integrators based on spectral deferred correction*, *SIAM Journal on Scientific Computing*, 42 (2020), pp. A1–A27.
- [11] T. BUVOLI, *Constructing polynomial block methods*, arXiv preprint arXiv:2011.00671, (2020).
- [12] T. BUVOLI, *Codebase for “Additive Integrators”*, (2021), <https://github.com/buvoli/apbm>.
- [13] T. BUVOLI, *Exponential polynomial block methods*, *SIAM Journal on Scientific Computing*, 43 (2021), pp. A1692–A1722.
- [14] T. BUVOLI AND M. TOKMAN, *Constructing new time integrators using interpolating polynomials*, *SIAM Journal on Scientific Computing*, 41 (2019), pp. A2911–A2937.
- [15] M. CALVO, J. DE FRUTOS, AND J. NOVO, *Linearly implicit runge-kutta methods for advection–reaction–diffusion equations*, *Applied Numerical Mathematics*, 37 (2001), pp. 535–549.
- [16] A. CARDONE, Z. JACKIEWICZ, A. SANDU, AND H. ZHANG, *Extrapolation-based implicit-explicit general linear methods*, *Numerical Algorithms*, 65 (2014), pp. 377–399.
- [17] A. CARDONE, Z. JACKIEWICZ, A. SANDU, AND H. ZHANG, *Construction of highly stable implicit-explicit general linear methods*, in *Conference Publications*, vol. 2015, American Institute of Mathematical Sciences, 2015, p. 185.
- [18] H. CHEN, *A splitting preconditioner for the iterative solution of implicit Runge-Kutta and boundary value methods*, *BIT Numerical Mathematics*, 54 (2014), pp. 607–621.
- [19] A. J. CHRISTLIEB, C. B. MACDONALD, AND B. W. ONG, *Parallel high-order integrators*, *SIAM Journal on Scientific Computing*, 32 (2010), pp. 818–835.
- [20] B. COCKBURN AND C.-W. SHU, *Runge-Kutta discontinuous Galerkin methods for convection-dominated problems*, *Journal of Scientific Computing*, 16 (2001), pp. 173–261, <https://doi.org/10.1023/a:1012873910884>.
- [21] E. M. CONSTANTINESCU AND A. SANDU, *Extrapolated implicit-explicit time stepping*, *SIAM Journal on Scientific Computing*, 31 (2010), pp. 4452–4477.
- [22] G. COOPER AND A. SAYFY, *Additive methods for the numerical solution of ordinary differential equations*, *Mathematics of Computation*, 35 (1980), pp. 1159–1172.
- [23] G. DIMARCO AND L. PARESCHI, *Implicit-explicit linear multistep methods for stiff kinetic equations*, *SIAM Journal on Numerical Analysis*, 55 (2017), pp. 664–690.
- [24] A. DUTT, L. GREENGARD, AND V. ROKHLIN, *Spectral deferred correction methods for ordinary differential equations*, *BIT Numerical Mathematics*, 40 (2000), pp. 241–266.
- [25] P. E. FARRELL, R. C. KIRBY, AND J. MARCHENA-MENENDEZ, *Irksome: Automating runge-kutta time-stepping for finite element methods*, arXiv preprint arXiv:2006.16282, (2020).
- [26] R. GLANDON, M. NARAYANAMURTHI, AND A. SANDU, *Linearly implicit multistep methods for time integration*, arXiv preprint arXiv:2011.10685, (2020).
- [27] E. HAIRER, S. P. NØRSETT, AND G. WANNER, *Solving ordinary differential equations I: Nonstiff problems*, *Siam Review*, 8 (1993), p. 528.
- [28] E. HAIRER AND G. WANNER, *Stiff differential equations solved by radau methods*, *Journal of Computational and Applied Mathematics*, 111 (1999), pp. 93–111.

- [29] G. IZZO AND Z. JACKIEWICZ, *Highly stable implicit–explicit runge–kutta methods*, Applied Numerical Mathematics, 113 (2017), pp. 71–92.
- [30] X. JIAO, X. WANG, AND Q. CHEN, *Optimal and low-memory near-optimal preconditioning of fully implicit runge-kutta schemes for parabolic pdes*, arXiv preprint arXiv:2012.12779, (2020).
- [31] C. A. KENNEDY AND M. H. CARPENTER, *Additive Runge–Kutta schemes for convection–diffusion–reaction equations*, Applied numerical mathematics, 44 (2003), pp. 139–181.
- [32] C. A. KENNEDY AND M. H. CARPENTER, *Higher-order additive runge–kutta schemes for ordinary differential equations*, Applied Numerical Mathematics, 136 (2019), pp. 183–205.
- [33] A. T. LAYTON AND M. MINION, *Implications of the choice of quadrature nodes for Picard integral deferred corrections methods for ordinary differential equations*, BIT Numerical Mathematics, 45 (2005), pp. 341–373.
- [34] M. MINION, *Semi-implicit spectral deferred correction methods for ordinary differential equations*, Communications in Mathematical Sciences, 1 (2003), pp. 471–500.
- [35] W. PAZNER AND P.-O. PERSSON, *Stage-parallel fully implicit Runge–Kutta solvers for discontinuous Galerkin fluid simulations*, Journal of Computational Physics, 335 (2017), pp. 700–717.
- [36] M. M. RANA, V. E. HOWLE, K. LONG, A. MEEK, AND W. MILESTONE, *A new block preconditioner for implicit runge-kutta methods for parabolic pde*, arXiv preprint arXiv:2010.11377, (2020).
- [37] A. SANDU AND M. GÜNTHER, *A generalized-structure approach to additive Runge–Kutta methods*, SIAM Journal on Numerical Analysis, 53 (2015), pp. 17–42.
- [38] L. F. SHAMPINE AND H. WATTS, *Block implicit one-step methods*, Mathematics of Computation, 23 (1969), pp. 731–740.
- [39] B. SOLEIMANI AND R. WEINER, *Superconvergent imex peer methods*, Applied Numerical Mathematics, 130 (2018), pp. 70–85.
- [40] B. S. SOUTHWORTH, O. A. KRZYSIK, AND W. PAZNER, *Fast solution of fully implicit Runge–Kutta and discontinuous Galerkin in time for numerical PDEs, part II: nonlinearities and DAEs*, arXiv preprint arXiv:2101.01776, (2021).
- [41] B. S. SOUTHWORTH, O. A. KRZYSIK, W. PAZNER, AND H. D. STERCK, *Fast solution of fully implicit Runge–Kutta and discontinuous Galerkin in time for numerical PDEs, part I: the linear setting*, arXiv preprint arXiv:2101.00512, (2021).
- [42] D. WANG AND S. J. RUUTH, *Variable step-size implicit-explicit linear multistep methods for time-dependent partial differential equations*, Journal of Computational Mathematics, (2008), pp. 838–855.
- [43] G. WANNER AND E. HAIRER, *Solving ordinary differential equations II*, Springer Berlin Heidelberg, 1996.
- [44] N. J. ZABUSKY AND M. D. KRUSKAL, *Interaction of solitons in a collisionless plasma and the recurrence of initial states*, Phys. Rev. Lett, 15 (1965), pp. 240–243.
- [45] H. ZHANG, A. SANDU, AND S. BLAISE, *High order implicit-explicit general linear methods with optimized stability regions*, SIAM Journal on Scientific Computing, 38 (2016), pp. A1430–A1453.

**SUPPLEMENTARY MATERIALS: ADDITIVE POLYNOMIAL  
METHODS, PART I:  
FRAMEWORK AND FULLY-IMPLICIT BLOCK METHODS \***

TOMMASO BUVOLI<sup>†</sup> AND BEN S. SOUTHWORTH<sup>‡</sup>

**SM1. IMEX-Radau and IMEX-Radau\*.** This section contains additional information about the polynomial IMEX-Radau and IMEX-Radau\* methods including: coefficients for methods with  $q = 3$  and  $q = 4$ , links to a code repository that contains scripts for deriving the coefficients for higher-order methods, and an additional stability figure for IMEX-Radau that is not contained in the paper.

**SM1.1. Coefficients for  $q = 2, 3, 4$ .** IMEX-Radau and IMEX-Radau\* propagator and iterator methods can be expressed as

$$(SM1.1) \quad \text{propagator:} \quad \mathbf{y}^{[n+1]} = \mathbf{A}\mathbf{y}^{[n]} + r\mathbf{B}^{\{1\}}\mathbf{f}^{\{1\}[n+1]} + r\mathbf{B}^{\{2\}}\mathbf{f}^{\{2\}[n]}$$

$$(SM1.2) \quad \text{iterator:} \quad \mathbf{y}^{[n+1]} = \tilde{\mathbf{A}}\mathbf{y}^{[n]} + r\mathbf{B}^{\{1\}} \left( \mathbf{f}^{\{1\}[n+1]} + \mathbf{f}^{\{2\}[n]} \right).$$

where the  $q \times q$  matrices  $\mathbf{A}$ ,  $\tilde{\mathbf{A}}$  are

$$(SM1.3) \quad A_{ij} = \begin{cases} 1 & j = q \\ 0 & \text{otherwise} \end{cases} \quad \tilde{A}_{ij} = \begin{cases} 1 & j = 1 \\ 0 & \text{otherwise} \end{cases}$$

and the  $q \times q$  matrices  $\mathbf{B}^{\{1\}}$ , and  $\mathbf{B}^{\{2\}}$  for  $q = 3, q = 4$  are

- $q = 2$  (for IMEX-Radau\* replace  $\mathbf{B}^{\{2\}}$  with  $\mathbf{B}^{*\{2\}}$ )

$$\mathbf{B}^{\{1\}} = \begin{bmatrix} 0 & 0 \\ 0 & 2 \end{bmatrix} \quad \mathbf{B}^{\{2\}} = \begin{bmatrix} 0 & 0 \\ 0 & 2 \end{bmatrix} \quad \mathbf{B}^{*\{2\}} = \begin{bmatrix} 0 & 0 \\ -1 & 3 \end{bmatrix}$$

- $q = 3$  (for IMEX-Radau\* replace  $\mathbf{B}^{\{2\}}$  with  $\mathbf{B}^{*\{2\}}$ )

$$\mathbf{B}^{\{1\}} = \begin{bmatrix} 0 & 0 & 0 \\ 0 & \frac{5}{3} & -\frac{1}{6} \\ 0 & \frac{3}{2} & \frac{1}{2} \end{bmatrix} \quad \mathbf{B}^{\{2\}} = \begin{bmatrix} 0 & 0 & 0 \\ 0 & -\frac{1}{6} & \frac{5}{6} \\ 0 & -\frac{3}{2} & \frac{7}{2} \end{bmatrix} \quad \mathbf{B}^{*\{2\}} = \begin{bmatrix} 0 & 0 & 0 \\ \frac{8}{27} & -\frac{11}{18} & \frac{53}{54} \\ \frac{4}{4} & -\frac{15}{2} & \frac{11}{2} \end{bmatrix}$$

\*Submitted to the editors DATE.

**Funding:** BSS was supported as a Nicholas C. Metropolis Fellow under the Laboratory Directed Research and Development program of Los Alamos National Laboratory.

<sup>†</sup>Department of Applied Mathematics, University of California, Merced, Merced CA 95343, USA. (tbuvoli@ucmerced.edu).

<sup>‡</sup>Theoretical Division, Los Alamos National Laboratory, USA (southworth@lanl.gov).

- $q = 4$  (for IMEX-Radau\* replace  $\mathbf{B}^{\{2\}}$  with  $\mathbf{B}^{*\{2\}}$ )

$$\mathbf{B}^{\{1\}} = \begin{bmatrix} 0 & 0 & 0 & 0 \\ 0 & \frac{1}{180}(88 - 7\sqrt{6}) & \frac{1}{900}(296 - 169\sqrt{6}) & \frac{2}{225}(-2 + 3\sqrt{6}) \\ 0 & \frac{1}{900}(296 + 169\sqrt{6}) & \frac{1}{180}(88 + 7\sqrt{6}) & \frac{1}{225}(-2)(2 + 3\sqrt{6}) \\ 0 & \frac{8}{9} - \frac{1}{3\sqrt{6}} & \frac{1}{18}(16 + \sqrt{6}) & \frac{2}{9} \end{bmatrix}$$

$$\mathbf{B}^{\{2\}} = \begin{bmatrix} 0 & 0 & 0 & 0 \\ 0 & \frac{1}{180}(-272 + 113\sqrt{6}) & \frac{1}{900}(296 - 169\sqrt{6}) & \frac{2}{225}(223 - 72\sqrt{6}) \\ 0 & \frac{1}{900}(296 + 169\sqrt{6}) & \frac{1}{180}(-272 - 113\sqrt{6}) & \frac{2}{225}(223 + 72\sqrt{6}) \\ 0 & \frac{1}{18}(-56 + 41\sqrt{6}) & \frac{1}{18}(-56 - 41\sqrt{6}) & \frac{74}{9} \end{bmatrix}$$

$$\mathbf{B}^{*\{2\}} = \begin{bmatrix} 0 & 0 & 0 & 0 \\ \frac{1}{500}(-1091 + 424\sqrt{6}) & \frac{1}{360}(-1198 + 517\sqrt{6}) & \frac{32402 - 14053\sqrt{6}}{9000} & \frac{12193 - 4152\sqrt{6}}{4500} \\ \frac{1}{500}(-1091 - 424\sqrt{6}) & \frac{32402 + 14053\sqrt{6}}{9000} & \frac{1}{360}(-1198 - 517\sqrt{6}) & \frac{12193 + 4152\sqrt{6}}{4500} \\ -16 & \frac{5}{18}(8 + 37\sqrt{6}) & \frac{1}{18}(-5)(-8 + 37\sqrt{6}) & \frac{122}{9} \end{bmatrix}$$

For larger  $q$  the coefficients can be obtained using the MATLAB script that found in the repository <https://github.com/pipack/paper-additive-pbms>. For convenience we also include the script in [subsection SM1.4](#).

**SM1.2. Additional stability regions for IMEX-Radau.** In Figure [SM1](#) we show stability regions for a composite IMEX-Radau method with  $q = 4$ . These can be directly compared with the stability regions for the composite IMEX-Radau\* with  $q = 4$  that are shown in Figure [??](#). In short we can see that the higher-order polynomial approximation used by IMEX-Radau\* for the explicit component leads to decreased in stability.

**SM1.3. Van Der Pol Results for IMEX-RK.** This subsection contains additional convergence diagrams for IMEX-Radau and IMEX-RK method on the Van der Pol equation. These diagrams supplement those shown in Figure [??](#). In Figure [SM3](#) we show four additional figures for IMEX-Radau, and in Figure [SM2](#) we show the corresponding diagrams for IMEX-RK methods. The results clearly demonstrate the superior stability properties of the IMEX-Radau methods for the linearly implicit splitting when  $\epsilon$  is small.



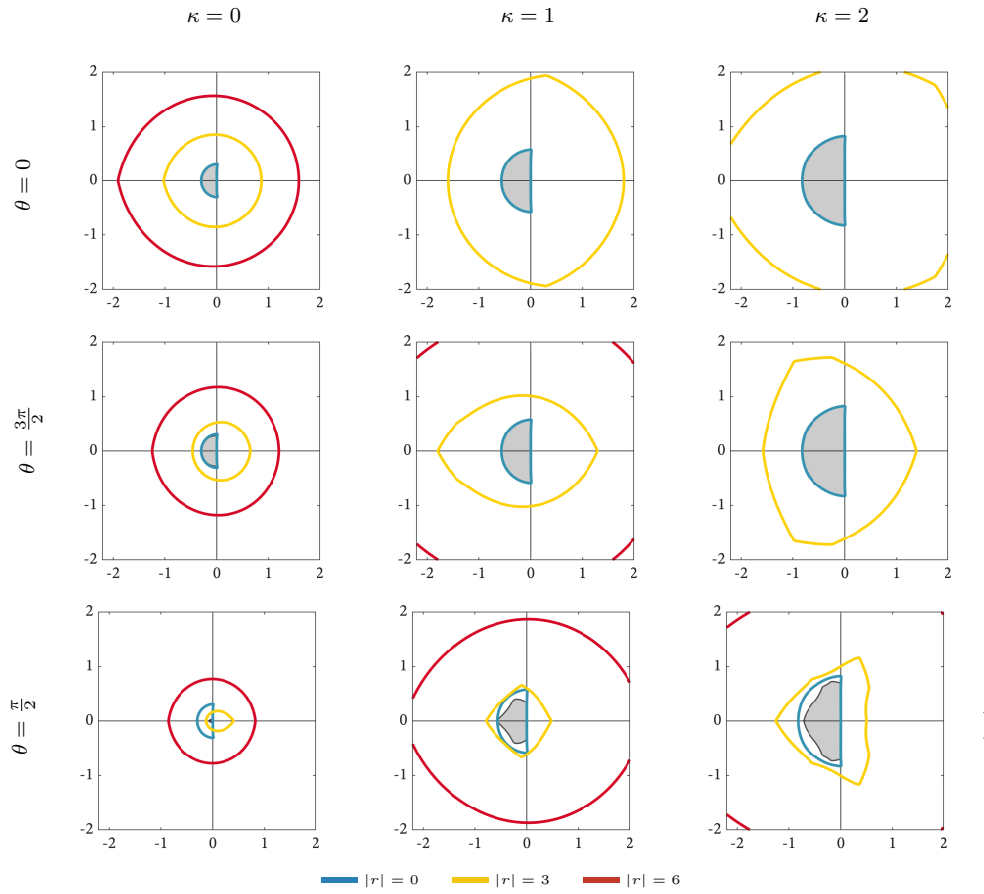


FIG. SM1. Stability regions for composite IMEX-Radau with  $q = 4$ . Each colored contour represents a different stability region  $R_{r,\theta}$  defined in (?). The gray region is the stability region  $R_\theta$  described in (?).

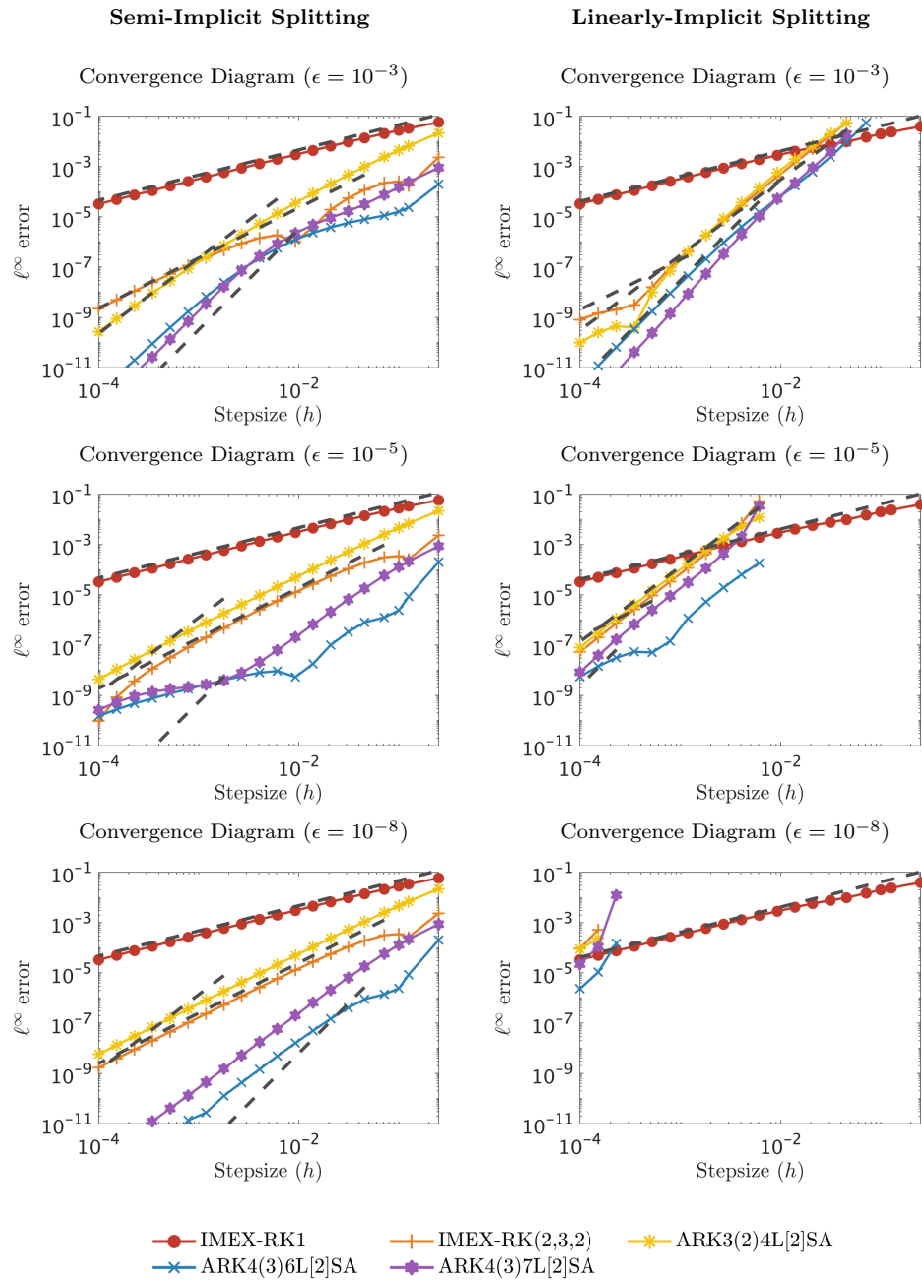


FIG. SM2. Four example convergence diagrams for IMEX-RK methods on the Van der Pol equation using the semi-implicit and linearly implicit splittings. IMEX-RK methods require very small timesteps to remain stable when using the linearly-implicit splitting for small  $\epsilon$ .

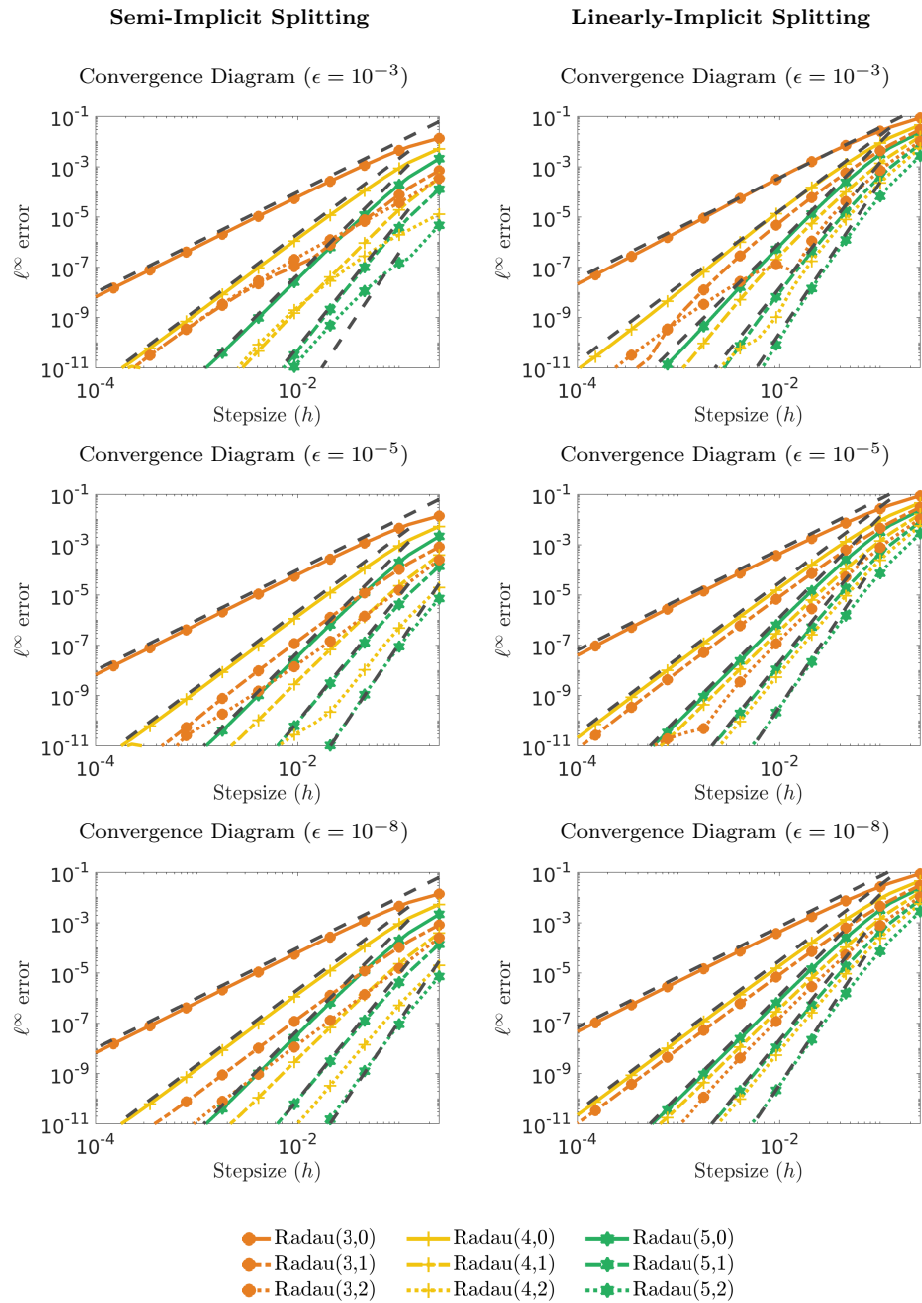


FIG. SM3. Four convergence diagrams for IMEX-Radau methods on the Van der Pol equation using the semi-implicit and linearly implicit splittings. The diagrams for  $\epsilon = 10^{-3}$  are identical to those shown in Figure ??.



**SM1.4. Matlab Script for Radau Coefficients.**

```

function [Bi, Be] = radauCoeff(q, star)
    if nargin == 1
        star = false;
    end

    Bi = zeros(q);
    Be = zeros(q);
    z = nodes(q);
    Bi(:,2:end) = transpose(quadW(z(2:end), z(1) * ones(q,1), z));
    if star
        Be = transpose(quadW(z, z(q) * ones(q,1), z + 2));
    else
        Be(:,2:end) = transpose(quadW(z(2:end), z(q) * ones(q,1), z + 2));
    end
end

function w = quadW(x, a, b)
%QUADW Returns quadrature weights for the nodes x where
%
%  $\int_a^b f(x) dx \approx \sum_{j=1}^n w(j,i) f(x(i))$ 
%
% == Parameters =====
% x (vector) - nodes
% a (vector) - left endpoints
% b (vector) - right endpoints
% =====

V = transpose(fliplr(vander(x)));
p = (1:length(x))';
b = ((b(:))'.^p - (a(:))'.^p) ./ p;
w = V \ b;
end

function z = nodes(q)
%QUADW Returns nodes for radau method
% == Parameters =====
% q (vector) - right endpoints
% =====

if(q > 8) % use chebfun if q > 8
    if(isempty(which('radaupts')))
        error('q > 8 requires Chebfun (https://www.chebfun.org/'));
    end
    z = [-1; -flip(radaupts(q-1))];
    return;
end

nodes = {
    [1]'

```

SUPPLEMENTARY MATERIALS: ADDITIVE POLYNOMIAL BLOCK METHODS SM7

```
[-0.3333333333333333, 1]'  
[-0.689897948556636, 0.289897948556636, 1]'  
[-0.822824080974592, -0.181066271118531, 0.575318923521694, 1]'  
[-0.885791607770965, -0.446313972723752, 0.167180864737834, ...  
0.720480271312439, 1]'  
[-0.920380285897062, -0.603973164252784, -0.124050379505228, ...  
0.390928546707272, 0.802929828402347, 1]'  
[-0.941367145680430, -0.703842800663031, -0.326030619437691, ...  
0.117343037543100, 0.538467724060109, 0.853891342639482, 1]'  
};  
z = [-1; nodes{q-1}];  
  
end
```